

PAPER

[View Article Online](#)
[View Journal](#) | [View Issue](#)



Cite this: *Environ. Sci.: Atmos.*, 2023, **3**, 1090

Dispersion of PM and VOC pollutants from open burning of municipal solid wastes on host communities: emission inventory estimation and dispersion modelling study

Adewemimo Oluwakunmi Popoola,^{*a} Lukuman Adekilekun Jimoda,^a
 Olusesan Abel Olu-Arotiowa,^a Oyetola Ogunkunle,^{ib}^{*b}
 Opeyeolu Timothy Laseinde,^b Sunday Adekunle Adebajo^c and Wuraola Abake Raji^d

The emissions from open burning of municipal solid wastes (MSWs) are very harmful. Owing to the scarcity of information on the impact of open burning of MSW on the onsite workers and the population within the vicinity of the Sokoto-Aiyekale dump site in Ilorin, Kwara State, this study focused on examining the impact of open burning of solid waste at the dump site on its host communities. The criteria air pollutants (CAPs) such as particulate matter (PM) and volatile organic compounds (VOCs) were determined using the emission factor approach. Deposition gauges were deployed at selected sampling spots to collect particulates which were characterized for heavy metal concentrations for the wet and dry seasons using energy dispersive X-ray fluorescence (EDXRF). The seasonal deposition fluxes, the deposition velocities and the scavenging ratios of the elements were estimated. The ground level concentrations of each of the CAPs within a 15 km radius were predicted using the AERMOD software (Version 8.2.0). The results showed that the emission inventory for PM and VOCs is in the range of 2200.5–2481.1 and 5913.9–6668.0 tons per annum between 2016 and 2020, respectively. Fourteen elements (Fe, Au, Ag, Pd, Rh, Cd, Zn, In, Sn, Cu, Mn, Ti, Ru, and S) were identified from the deposition study, with Fe having the highest concentration of 67 512.8 and 73 845.5 $\mu\text{g m}^{-3}$ in the wet and dry seasons, respectively. The wet and dry deposition fluxes ranged from 7.32 to 11.46 and 38.83 to 88.8 g per m^2 per month, respectively. Deposition velocities of the trace metals were in the range of 0.0000528–0.00075444 and 0.0003377–0.0048183 m s^{-1} in the wet and dry seasons, respectively. The average 1, 8, 24 h, and annual concentrations were 16 175, 6634, 3190 and 409 $\mu\text{g m}^{-3}$ for PM and 20 959, 7000, 3700 and 418 $\mu\text{g m}^{-3}$ for VOCs, respectively. This research shows that open burning of solid wastes is characterized by harmful gaseous emissions and heavy metals with potential adverse effects on receptor communities. These findings will serve as baseline information for environmental protection agencies.

Received 21st March 2023
 Accepted 15th May 2023

DOI: 10.1039/d3ea00041a

rsc.li/esatmospheres

Environmental significance

This research investigated the emissions from open burning of solid waste at the Sokoto-Aiyekale dump site. The ground level concentrations of criteria air pollutants were estimated using AERMOD. The criteria air pollutants (CAPs) such as particulate matter (PM) and volatile organic compounds (VOCs) were determined using the emission factor approach. This study established the fact that anthropogenic activities such as open burning of solid waste produce heavy metals in large concentrations, which has a negative impact on the environment. Baseline data were generated which can be adopted by the Federal Ministry of Environment and Environmental Protection Agency. This research provided a template for stakeholders in the environmental sector to take appropriate measures to attenuate the effects of open burning of solid waste on human health and the environment.

1. Introduction

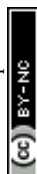
With the increase in human population and the non-stop generation of solid wastes on a daily basis, so is the corresponding magnitude and variety of wastes contending for space with men and its effect impairing the quality of the environment.¹ As much as one billion tonnes of wastes, equivalent to about half of all the municipal solid wastes generated on Earth

^aDepartment of Chemical Engineering, Ladoke Akintola University of Technology, Oyo State, Nigeria. E-mail: aopopoola95@lautech.edu.ng

^bDepartment of Mechanical and Industrial Engineering Technology, University of Johannesburg, South Africa. E-mail: oogunkunle@uj.ac.za

^cDepartment of Chemical and Polymer Engineering, Lagos State University, Nigeria

^dDepartment of Chemical and Petroleum Engineering, Igbinedion University, Okada, Nigeria



are burnt in open and uncontrolled fires around the world annually.² Because of the release of a hazardous cocktail of emissions into the atmosphere and onto land, the impact on human health and the environment is likely to be severe, posing risks to populations, workers, and the environment.³

Different types of materials are classified as municipal solid waste (MSW). These include refuse, sludge from a waste treatment plant, air pollution control facility and other discarded materials such as solid, liquid, semisolid, and/or gaseous materials resulting from industries. Waste from institutions such as schools and hospitals, community activities, as well as commercial sources, such as restaurants and small businesses, mining and agricultural operations, are also regarded as MSW.⁴ The rate and quantity of waste generation have recently increased. As the quantity of waste increases, so does the variety.⁵ As opposed to the prehistoric period, when wastes were merely a nuisance that had to be disposed, proper management was not a major concern because of the small number of people and a vast amount of land was available to the population at the time. During this period, the environment readily taken up by the amount of waste produced without any degradation.⁶

The World Bank predicts that waste generation will increase from 2.01 billion tonnes in 2016 to 3.40 billion tonnes in 2050. At least 33% of this waste is currently mismanaged globally through open dumping or burning.⁷ The rise in waste generation rate will result in an increase in environmental challenge if not effectively managed. Global MSW data revealed a generation rate of 0.68 billion tons per year in 2000 and 1.3 billion tons per year in 2010, with an estimated 2.2 billion tons per year in 2025 and 4.2 billion tons per year in 2055.⁸ Today, the rate at which waste is being generated is about 70% as compared to the total rate of its disposal which is 30%.⁹ Municipal solid waste management (MSWM), a vital feature in achieving sustainable metropolitan growth, entails the separation, storage, collection, relocation, processing, and disposal of solid waste in order to reduce its environmental impact. Unmanaged MSW contributes to the spread of numerous diseases.¹⁰ The earth is very good at resource recovery, but when the quantity of waste generated exceeds its capacity, it presents a serious threat to lives, a concept known as pollution, which occurs at varying concentrations and affects all forms of life.¹¹

The global public health crisis is being exacerbated by dirty air. Over 90% of the global population lives in areas where air pollution exceeds World Health Organization standards.¹² Some scientific studies have found a link between the formation of PM and VOC emissions.¹³ Shao *et al.*¹³ reported that VOCs play an important role in the formation of PM and oxidants, contributing to summertime air pollution under certain humid conditions. Their report suggested that some VOC groups may promote an increase in PM concentrations unless PM levels exceed $140 \mu\text{g m}^{-3}$ under humid conditions.

Particulate matter (PM) refers to all solid and liquid particles suspended in air, many of which are hazardous.¹⁴ Particulate matter is a broad term used to describe air pollutants that consist of suspended particles in the air that vary in composition and size as a result of various anthropogenic activities.¹⁵ The size, composition, and the concentration of the particulate

matter depend on the type of gasifier and its operating conditions such as temperature, gas velocity, moisture content in fuels, and rate of gasification. The size of the particulate matter varies from less than 1 micron to larger than 100 microns. Besides posing health risk, particulate matter is also responsible for causing fouling, erosion, and corrosion of downstream equipment.¹⁶ Particulate matter is the main contributor for air pollution. It decreases the clarity in air and therefore affects the visibility and makes it difficult to breathe such air.¹⁷ Particulate matter includes all solid and liquid particles that are found in the suspended condition in air. Many of them are usually hazardous and act as major risk factors for imposing much comorbidity in humans.¹⁸

Volatile organic compounds (VOCs) are gaseous chemicals emitted into the atmosphere by many of the solid or liquid products we use to build and maintain our homes.¹⁹ Volatile organic compounds have a high vapor pressure but a low water solubility. VOCs contain a wide range of chemicals, some of which may have short- and long-term negative health effects. Many VOC concentrations are consistently up to ten times higher indoors than outdoors.²⁰ Once in the air, some can react with other gases to form other air pollutants. Some are toxic, including those that cause cancer and other health related issues.²¹ VOCs can be found in both indoor and outdoor air. Some of the more well-known VOCs are benzene, formaldehyde, and toluene. VOCs can irritate the eyes, nose, and throat, cause difficulty in breathing and nausea, and damage the central nervous system and other organs when inhaled. Some VOCs have been linked to cancer.¹⁹

Using mathematical formulations, air dispersion of a pollutant emitted by a source can be modelled.²² Vallero²³ suggested that dispersion models can be used to estimate the distribution of pollutants in the atmosphere based on the emissions from a source and the atmospheric conditions. These models are commonly used to predict the concentration of pollutants at various downwind receptor locations. These models are commonly used in the management of the environmental impact of pollutant emissions. Air dispersion modelling is a widely used tool for managing the impacts of pollutant emissions on the environment. As Ryan and LeMasters²⁴ noted, these models are commonly used for various purposes, such as environmental impact assessments, risk analysis, emergency planning, and source apportionment studies. The models estimate the dispersion of pollutants in the atmosphere and help to assess the potential impacts on human health and the environment. Air dispersion models play a significant role in the policy and decision-making process. By providing information on the potential impacts of emissions, they help policymakers and decision-makers to make informed choices about environmental policies and regulations, such as setting emission limits and establishing air quality standards. These models also assist in identifying areas where air quality management efforts are needed and can be used to evaluate the effectiveness of different mitigation strategies.

Open waste burning is common practice in low- and middle-income countries, but systematic and modelling studies and evidence of the practice are lacking.²⁵ The scientific foundation



for modelling the impact of emissions from open burning is also lacking. Exposure to open waste burning was found to pose the greatest risk to human and environmental health of all waste categories and disposal methods studied.³ This work was limited to the Kwara State Government approved dump site located at Sokoto Aiyekale, along the Jebba-Bode Sadu Road in Ilorin. It involves the estimation of the emission inventory from 2016 to 2020, determination of heavy metals in the ambient air through wet and dry deposition and forward trajectory modelling of the pollutants resulting from the combustion activities using AERMOD.

2. Research methodology

This case study centred on the dispersion of pollutants (PM and VOCs) generated from the open burning of solid waste. The Industrial Source Complex Short Term Version 3 model, which is included in the United States Environmental Protection Agency (USEPA) Regulatory Model, AERMOD View software, was employed in the dispersion simulations of pollutants. It was used to predict the change in ground-level air quality associated with the study area at communities within a defined radius of the location to the source of the pollutants. Its uses include a wide range of options for modelling air quality impact of pollution sources. It uses the pathway that composes the run stream file as the basis for its functional organization. These pathways include Control Pathway (CO), Source Pathway (SO), Receptor Pathway (RE), Meteorological Pathway (ME), Terrain

Grid Pathway (TG), and Output Pathway (OU).²⁶ This model has two pre-processors: namely, a meteorological data pre-processor called AERMET, which calculates the boundary-layer meteorological parameters (such as wind speed, wind direction, temperature, and cloud cover), and prepares these data in a format readable by AERMOD, and a terrain data pre-processor called AERMAP, which designates the elevation of the receptor grid and generates gridded terrain data.²⁷

2.1 Study area

The research site is a 600-plot (390 000 sqm) government-approved disposal site with 130 burning points in Aiyekale, Ilorin, Kwara State (Fig. 1 and 2), within latitude 8° 28'N and longitude 4° 27'E. It is approximately 500 kilometers from Abuja, Nigeria's Federal Capital, and is strategically located at the geographical and cultural crossroads of Northern and Southern Nigeria. The geological setting of the city indicates that Aiyekale is underlain by the Precambrian basement complex comprising acidic rocks such as granite and rhyolite. The city (Ilorin) serves as the state capital and headquarters for its three local government areas. The city can be classified into three sub-areas: commercial/industrial areas, old residential area, and government reservation area.²⁸ The city's demographic growth over time is responsible for the city's continuous rise in MSW generation rate as well as its consequences. The city's core includes the Emir's palace, the Central Mosque, and the Emir's market.⁸

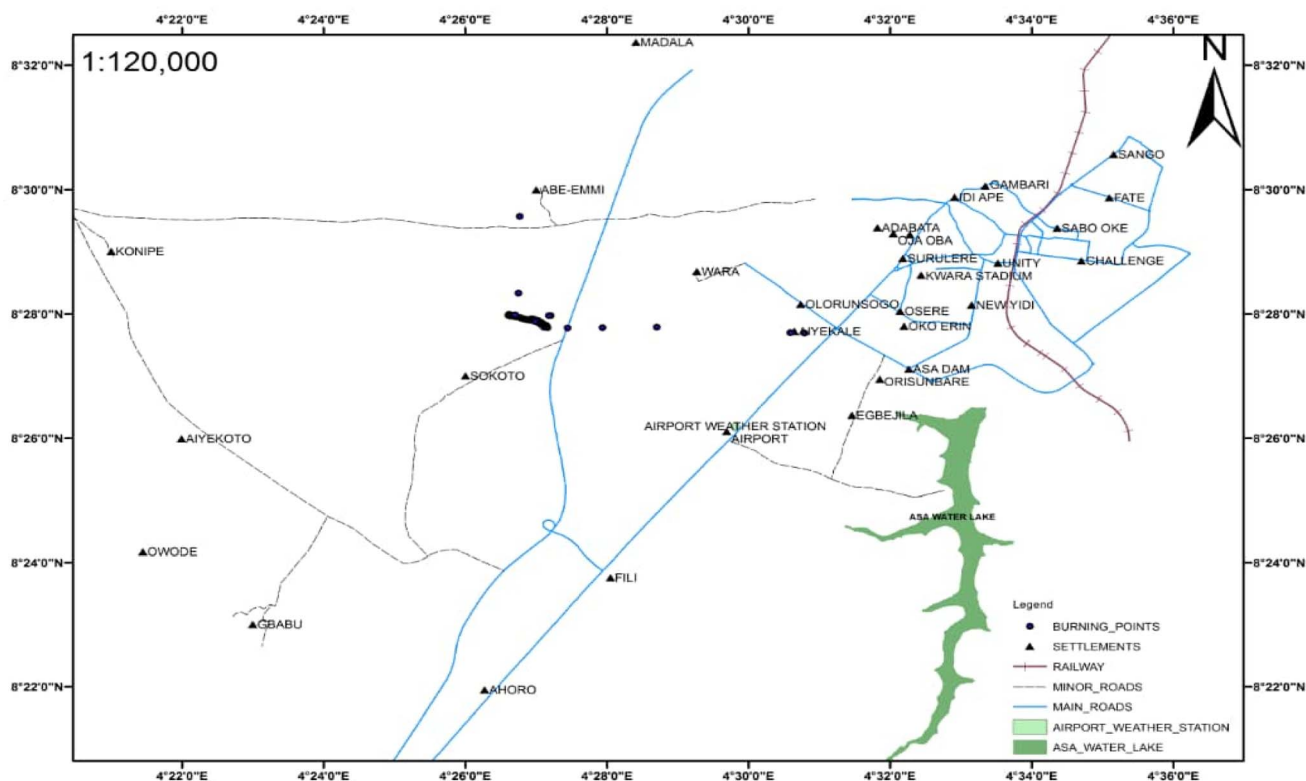


Fig. 1 Study area located in Aiyekale, Ilorin, Kwara State. Source: Google Earth (2022).





Fig. 2 Picture of the Sokoto-Aiyekale dump Site. Source: Authors fieldwork (2022).

The indigenous area of town, known as the old residential area, is located in the central core area. The post-colonial area located around the city's core is the new residential area, whereas the government reserved area is the elevated neighbourhood area. Sobi Hill is an isolated hill in the city with an elevation of 394 m above sea level (ASL) in the north-western part and 200 m to 346 m in the east. Ilorin's drainage system has a dendritic pattern.²⁸ The wet season runs from March to October, and the dry season runs from November to February. The city's average annual rainfall is 1200 mm.²⁹ The government of Kwara State approved a bill in 2015 authorizing that all defunct landfilling locations within the city be demolished in order to make for growth and urbanization in the state, because it is an absolute mess for a state capital to have huge amounts of open refuse landfills on every accessible space on the road and street.

2.2 Emission inventory estimation

This work adopted the emission estimation techniques (EETs) to determine the amount of PM and VOC emissions due to open burning of the waste. The quantity of air pollutants emitted from the open burning of solid waste in the Sokoto-Aiyekale dumpsite, Ilorin, Nigeria was determined using the emission factor approach. Using eqn (1) reported by Sonibare,³⁰ emission rates of air pollutants (PM and VOCs) from the open burning of solid waste were calculated. Daily, weekly, monthly and annual emissions were estimated based on the amount of solid waste burned and equivalent emission factors for each pollutant. Different solid waste types and combustion conditions could generate different emission factors in different countries. However, these emission factors for different air pollutants are taken to be the same globally, irrespective of the country.

The emission factor used for the PM and VOC emissions from municipal solid waste combustion was adopted from the United States Environmental Protection Agency. The AP-42 compilation of air pollutant emissions developed by the United States Environmental Protection Agency (USEPA)³¹ states that the emission factor of PM and VOCs for municipal solid

waste combustion is 8 kg Mg^{-1} and 21.5 kg Mg^{-1} , respectively. It simply implies that for municipal solid waste combustion, the estimated amount of particulate matter emission is 8 kg Mg^{-1} of the quantity of solid waste combusted. Also, to estimate the quantity of VOCs emitted, an emission factor of 21.5 kg of VOCs per kg of the quantity of municipal solid waste combusted was considered. The word estimate here means an approximate value (plus or minus) given by USEPA.

Criteria air pollutant emitted in ton per year

$$= \frac{\text{emission factor (kg) of pollutant}}{1 \text{ Mg of solid waste burnt}} \times \frac{1 \text{ Mg}}{1000 \text{ kg}} \times \text{yearly solid waste generated} \quad (1)$$

For year 2016,

$$\begin{aligned} \text{Daily PMs emission (g)} &= \frac{\text{emission factor (kg) of PMs}}{1 \text{ Mg of solid waste burnt}} \\ &\times \frac{1 \text{ Mg}}{1000 \text{ kg}} \times \text{daily solid waste generated in 2016} \end{aligned} \quad (2)$$

$$\text{Weekly PM emission (g)} = \text{daily PM emission (g)} \times 7 \quad (3)$$

$$\text{Monthly PM emission (g)} = \text{daily PM emission (g)} \times 30 \quad (4)$$

$$\text{Annual PM emission (g)} = \text{daily PM emission (g)} \times 365 \quad (5)$$

$$\begin{aligned} \text{Daily VOCs emission (g)} &= \frac{\text{emission factor (kg) of VOCs}}{1 \text{ Mg of solid waste burnt}} \\ &\times \frac{1 \text{ Mg}}{1000 \text{ kg}} \times \text{daily solid waste generated in 2016} \end{aligned} \quad (6)$$

$$\text{Weekly VOC emission (g)} = \text{daily VOC emission (g)} \times 7 \quad (7)$$

$$\text{Monthly VOC emission (g)} = \text{daily VOC emission (g)} \times 30 \quad (8)$$

$$\text{Annual VOC emission (g)} = \text{daily VOC emission (g)} \times 365 \quad (9)$$

The daily, weekly, monthly and annual CAPs for year 2017 to 2020 were estimated using eqn (2)–(9).

2.3 Estimation of deposition velocities of heavy metals using deposition flux measurement

The deposition flux measurements were carried out for both wet and dry seasons using deposition gauges according to Adebajo *et al.*³² To measure the flux of settleable particulate matter, ten deposition gauges (0.2 m diameter by 0.15 m depth) were placed at strategic locations throughout the study area. During the sampling period, the gauges were left permanently for one month.³³ Rainwater and sediments were collected and filtered for wet deposition using a digital weighing balance and dry pre-



weighed Whatman (125 mm diameter) filter paper (model PA2102). The filter papers were then dried in a glass box to prevent further particle settlement. The filter paper and particles were then reweighed in order to calculate the total particle mass collected. For dry deposition, the gauges were also planted for a month as done in the wet season. Since it is a dry season, it was expected that the particles in the gauges will be dried. After rinsing the deposition gauges with distilled water to remove all of the deposited matter, the water was drained and filtered through a dry pre-weighed filter. The filtered papers were then dried and reweighed in a desiccator.

2.3.1 Measurement of wet and dry deposition flux. The wet and dry deposition flux rates were determined using eqn (10) according to Jimoda *et al.* (2010).³³

$$\text{Deposition flux} = \frac{W_p}{A \times t} \quad (10)$$

where W_p = weight of particulate matter (g); A = area of the deposition gauges (m^2); t = duration of exposure (month).

2.3.2 Heavy metal characterization in deposited PM. Using energy dispersive X-ray fluorescence (EDXRF) spectrometry, the deposited matter was analyzed for heavy metals. All measurements were performed with a Model XR-100CR, a high-performance X-ray detector with a preamplifier and a cooler system that uses a thermoelectrically cooled Si-PIN photodiode as an X-ray detector. Because of its high sensitivity, which measures to parts per million of a gram in a sample, the EDXRF was used for this analysis. It also functions as a multi-element detector. The elements detected are iron (Fe), gold (Au), silver (Ag), palladium (Pd), rhodium (Rh), cadmium (Cd), zinc (Zn), indium (In), tin (Sn), tungsten (W), copper (Cu), manganese (Mn), titanium (Ti), ruthenium (Ru) and sulphur (S).

2.3.2.1 Analysis instrumentation. The instrument to be used for this analysis is an energy dispersive X-ray fluorescence (EDXRF) spectrometer. The X-ray spectrum emitted by a solid sample bombarded with a focused beam of electrons is used in this method to obtain a localized chemical analysis.³⁴ In concept, all elements with atomic numbers ranging from 4 (Be) to 92 (U)

2.3.2.2 Sample preparation. The samples were dried, crushed, and grinded before being analyzed. The samples were pelletized using steel molds, pellets, and a hydraulic press, with aluminium foil used as a binding material to keep the sample particles together after they were removed from the molds. This was followed by sample irradiation, which is discussed further below.

2.3.2.3 Sample irradiation. The sample chamber was filled with irradiated samples. The sample chamber is connected to the source X-ray tube and the Si-PIN photodiode detector, which are both at 45° to it. The source X-ray tube was set to 25 kV and a current of 50 μA , and each sample was irradiated for 1000 seconds. The actual time spent is determined by the electronic system. The real time (RT) is the amount of time it takes for the electronic system and the X-ray photon signals reproduced from the fluorescing atoms in the samples to detect the photon energy, which is usually longer than the pre-set 1000 seconds. The sample fluorescence should emit characteristic X-rays of the absorbing atoms from which the X-ray photons are ejected. The photons ejected are from the quantum physical electronic transition between the K and L shells, which produces $K(\alpha)$ radiation, and the one between the K and M shells, which produces $K(\beta)$ radiation. The energy difference between the K-L shell and K-M shell electron transitions emits photons that appear to be reflected in the form of an increase in the wavelength of the detected X-rays. These detected photon energies are signatures for known elements with standard experimental energies against which the detected energies for each atom in the sample are compared. The detector detects the emitted photons and sends their corresponding signal currents to the preamplifier. The signal is converted to data by the multi-channel analyzer and then sent to the quantitative analysis software package.

2.3.3 Evaluation of deposition velocities and scavenging ratios of the heavy metals. The heavy metal deposition velocities in the study area were calculated using eqn (11) as the flux per concentration of trace metals precipitated.³³

$$\text{Deposition velocities} = \frac{\text{deposition flux}}{\text{concentration of the trace metals precipitated}} \quad (11)$$

can be identified. Qualitative analysis involves identifying the lines in the spectrum and is relatively simple due to the simplicity of X-ray spectra. The qualitative approach (identifying element concentrations) involves measuring line intensities for each element in the sample as well as the same elements in known composition calibration standards.³⁵ For the 5.9 keV peak of ^{55}Fe , the detector resolution is 220 eV FMHM with a shaping time constant of 12 μs for the standard setting and 186 eV FMHM with a shaping time constant of 20 μs for the optional setting. The XRF-FP qualitative analysis software package was used to analyze the samples qualitatively. This converts elemental peak intensities into concentrations or film thicknesses.

The scavenging ratio of heavy metals is of importance in the understanding of the influence of deposition on the lifetime of the heavy metals in the environment. Under the approximation that the concentration of pollutants in precipitation (C_p) depends on the concentration in the air (C_A) within which precipitation is formed,³⁶ the scavenging ratio (SR) is expressed as shown in eqn (12).

$$\text{Scavenging ratio (SR)} = \frac{C_p}{C_A} \quad (12)$$

where C_p = concentration of heavy metals in the precipitate; C_A = concentration of heavy metals in the air.



2.4 Dispersion modelling

According to Amouzouvi *et al.*³⁶ the spatial dispersion was modelled using the American Meteorological Society/Environmental Protection Agency Regulatory Model (AERMOD). It uses two preprocessors (AERMET and AERMAP), which uses terrain and meteorological data to produce suitable input data for AERMOD. Air quality modeling is a fundamental tool for determining the spatial distribution of overall pollutant concentrations. AERMOD was used to estimate the ground level concentrations of each identified CAP and to predict the change in ground level air quality within a 15 kilometer radius of the pollutant source. It bases its functional organization on the pathways that comprise the run stream file. The modelling procedure was as follows:

2.4.1 Meteorological pathway. The atmospheric conditions of the area to be modelled were defined here so that they could be taken into account when determining the distribution of air pollution impacts for the area.

2.4.2 Control pathway. The modelling scenario and overall modelling run control such as the pollutants and averaging periods were specified here.

2.4.3 Source pathway. The source pathway is where sources of pollutants emission being modelled were defined. It gives information on the number of emission sources and pollutants specified.

2.4.4 Receptor pathway. This is where the receptors at specific locations are specified for the purpose of determining the air quality impact.

2.4.5 Terrain grid pathway. This is where the gridded terrain data to be used in calculating dry depletion in elevated or complex terrain are specified.

2.4.6 Output pathway. This is where the output results necessary to meet the needs of the air quality modelling analysis were determined. The resultant output was the ground level concentration of pollutants modelled. A uniform Cartesian coordinate was considered for the receptor pathway. A scaled map (length, breadth and scale length of the map measured) of the location was imported to the site domain where the size of the domain was specified as the *X* and *Y* coordinates for the two points, the southwest (SW) point (min.) and the northwest (NW) point (max.) of the domain. The receptor locations obtained from the map, emission sources, emission rates and meteorological data were inputted into the source dialog box. Then, the dispersion model was run to obtain the ground level concentration of emission on the host environments in 1 h, 8 h, 24 h and annual averaging time.

3. Results and discussion

The results obtained in this research include solid waste composition, determination of solid waste generated from 2016 to 2020, emission inventory estimation, determination of deposition velocities of heavy metals using deposition flux measurement, estimation of scavenging ratios of the heavy metals and modelling of the air pollutants using AERMOD.

Table 1 PM and VOC emissions for 2016–2020

	2016			2017			2018			2019			2020		
	PM (g)	VOCs (g)		PM (g)	VOC (g)		PM (g)	VOC (g)		PM (g)	VOC (g)		PM (g)	VOC (g)	
Daily	6 028 800	16 202 400		6 212 800	16 696 900		6 401 600	17 204 300		6 596 800	17 728 900		6 797 600	18 268 550	
Weekly	42 201 600	113 416 800		43 489 600	116 878 300		44 811 200	120 430 100		46 177 600	124 102 300		47 583 200	127 879 850	
Monthly	180 864 000	486 072 000		186 384 000	500 907 000		192 048 000	516 129 000		197 904 000	531 867 000		203 928 000	548 056 500	
Yearly	2 200 512 000	5 913 876 000		2 267 672 000	6 094 368 500		2 336 584 000	6 279 569 500		2 407 832 000	6 471 048 500		2 481 124 000	6 668 020 750	



3.1 Emission inventory estimation

The emission inventory of the PM and VOC emissions due to open burning of waste from 2016–2020 is presented in this section. According to USEPA,³⁰ the emission factors of PM and VOCs for municipal solid waste combustion were given to be 8 kg Mg⁻¹ and 21.5 kg Mg⁻¹ respectively. The daily/weekly/monthly/annual emissions were estimated based on the amount of solid waste burnt and equivalent emission factors for PM and VOCs.

Table 1 shows the PM and VOC pollutants emitted between 2016 and 2020. In 2016, the daily PM and VOCs emitted were calculated to be 6 028 800 g and 16 202 400 g respectively. The weekly values were 42 201 600 g and 113 416 800 g respectively. The monthly values were 180 864 000 g and 486 072 000 g respectively. The yearly values were calculated to be 2 200 512 000 g and 5 913 876 000 g respectively. In 2017, the daily PM and VOCs emitted were calculated to be 6 212 800 g and 16 696 900 g, respectively. The weekly values were 43 489 600 g and 116 878 300 g respectively. The monthly values were 186 384 000 g and 500 907 000 g respectively. The yearly values were calculated to be 2 267 672 000 g and 6 094 368 500 g respectively. In 2018, the daily PM and VOCs emitted were calculated to be 6 401 600 g and 17 204 300 g, respectively. The weekly values were 44 811 200 g and 120 430 100 g, respectively. The monthly values were 192 048 000 g and 516 129 000 g, respectively. The yearly values were calculated to be 2 336 584 000 g and 6 279 569 500 g, respectively. In 2019, the daily PM and VOCs emitted were calculated to be 6 596 800 g and 17 728 900 g, respectively. The weekly values were 46 177 600 g and 124 102 300 g, respectively. The monthly values were 197 904 000 g and 531 867 000 g, respectively. The yearly values were calculated to be 2 407 832 000 g and 6 471 048 500 g, respectively. In 2020, the daily PM and VOCs emitted were calculated to be 6 797 600 g and 18 268 550 g, respectively. The weekly values were 47 583 200 g and 127 879 850 g, respectively. The monthly values were 203 928 000 g and 548 056 500 g, respectively. The yearly values were calculated to be 2 481 124 000 g and 6 668 020 750 g, respectively.

Table 1 also shows that the emission of VOCs, which is the second highest of all the criteria air pollutants resulting from the combustion of solid waste. There is an increase in the VOC emission from 2016 to 2020 due to the increase in the generation of solid waste. From 2016 to 2020, VOCs increase from 16.2 to 18.3 tons per day, from 113.4 to 127.9 tons per week, from 486.1 to 548.1 tons per month and 5913.9 to 6668.0 tons per year. These values must be controlled because of the effects of volatile organic compounds which include damaging of the

audible and visual senses.³⁸ The average, standard deviation, and uncertainty values of daily/weekly/monthly/annual emissions of PM and VOCs are presented in Table 2.

Likewise, the result revealed that the emission of PM, which is the third highest of all the criteria air pollutants results from the combustion of solid waste. There is an increase in the PM emission from 2016 to 2020 due to the increase in the generation of solid waste. From 2016 to 2020, PM increases from 6.0 to 6.8 tons per day, from 42.2 to 47.6 tons per week, from 180.9 to 203.9 tons per month and 2200.5 to 2481.1 tons per year. Wheezing, aggravation of asthma, shortness of breath, coughing and chest pain are some of the short-term effects of particulate matter inhalation. Long-term exposure to particulate matter can result in heart failure, respiratory disease and lung cancer.³⁹ Children, the aged, and people with pre-existing respiratory conditions are mostly vulnerable to PM health impacts. Furthermore, pregnant mothers and their babies are at serious risk for mortality and health problems because of PM exposure.⁴⁰ The emission of PM from the combustion of solid waste must be attenuated.

3.2 Deposition fluxes at selected sampling spots

Deposition gauges were used to measure the deposition flux during both seasons. Deposition gauges were placed at strategic locations to monitor the flux of settleable particulate matter. For one month, the gauges were left permanently.

3.2.1 Wet and dry deposition flux distribution at selected sampling spots. The deposition fluxes of particulates collected at the study area in the wet season are summarized in Table 3. The values ranged from (7.32–11.46 g per m² per month), the highest flux (11.46 g per m² per month) was found at sampling spot 4, while sampling spot 5 recorded the lowest flux (7.32 g per m² per month). The deposition flux increases in the following order SS4 > SS2 > SS6 > SS8 > SS1 > SS9 > SS3 > SS7 > SS10 > SS5. The percentages of the deposition fluxes from sampling spot 1 to 10 were 10.3%, 11.7%, 9.3%, 12.4%, 7.9%, 11%, 8.6%, 10.7%, 9.9% and 8.2% respectively. In the dry season, the deposition fluxes of particulates at the study area ranged from 38.83–88.8 g per m² per month. The highest flux (88.8 g per m² per month) was obtained at sampling spot 9, while the lowest flux (38.83 g per m² per month) was recorded at sampling spot 3. The flux increases in the following order SS9 > SS10 > SS6 > SS4 > SS5 > SS7 > SS2 > SS8 > SS1 > SS3. The percentages of the deposition fluxes from sampling spot 1 to 10 were 7%, 8.3%, 6.6%, 10.9%, 10.3%, 12.2%, 8.9%, 7.3%, 15% and 13.5% respectively.

Table 2 The average, standard deviation, and uncertainty values of daily/weekly/monthly/annual emissions of PM and VOCs from 2016–2020

	Average		Std. Dev.		Uncertainty	
	PM	VOC	PM	VOC	PM	VOC
Daily	6 407 520	17 220 210	303 878.71	816 674.04	135 898.69	365 227.73
Weekly	44 852 640	120 541 470	2 127 150.99	5 716 718.28	951 290.84	2 556 594.14
Monthly	192 225 600	516 606 300	9 116 361.38	24 500 221.21	4 076 960.75	10 956 832.02
Yearly	2 338 744 800	6 285 376 650	110 915 730.10	298 086 024.70	49 603 022.46	133 308 122.90



Table 3 Wet and dry deposition fluxes at selected sampling spots

Sampling spot	Wet season (g per m ² per month)	Dry season (g per m ² per month)
1	9.55	41.37
2	10.82	48.70
3	8.59	38.83
4	11.46	64.61
5	7.32	60.47
6	10.18	71.93
7	7.96	52.51
8	9.87	42.97
9	9.23	88.80
10	7.64	79.89
Control	0.95	33.74

The deposition fluxes of the control site were lower than those of the sampling sites because no history of open burning is recorded at the control site which is 6 km away from the study area. The result showed that the wet season fluxes were lower than the dry season fluxes due to the high precipitation that washes down the particulates in the wet season which is not so in the dry season when we have more particles resuspended in the atmosphere thereby resulting in high deposition fluxes.⁴¹

3.2.2 Heavy metal characterization in deposited particulate matter. The concentration of each metal at the selected sampling spots is presented and discussed in this section. The presence of heavy metals such as Fe, Au, Ag, Pd, Rh, Cd, Zn, In, Sn, W, Cu, Mn, Ti, Ru and S was detected in the particulate matter collected at the sampling sites in both seasons. According to Nagpure *et al.*,⁴² open combustion of plastics, glass, metals and organic wastes results in the emission of metals. The United State Environmental Protection Agency (USEPA) and the World Health Organization (WHO) have respectively set 35 µg m⁻³ and 25 µg m⁻³ as the standard for metal emissions.

Iron (Fe) was predominantly high in all the sampling spots, which is similar to the result of Kumar *et al.*⁴³ However, the

highest concentration was recorded at sampling spot (SS) 2, as shown in Table 4 ($111.65 \times 10^3 \pm 5.575 \times 10^3 \mu\text{g m}^{-3}$) while the lowest concentration of $30.679 \times 10^3 \pm 4.222 \times 10^3 \mu\text{g m}^{-3}$ was recorded at SS 9. The dry season analysis reveals that the highest concentration of $117.369 \times 10^3 \pm 4.603 \times 10^3 \mu\text{g m}^{-3}$ was found at SS 2, while the lowest ($58.841 \times 10^3 \pm 4.613 \times 10^3 \mu\text{g m}^{-3}$) was found at SS 4 (Table 5). The concentrations during the two seasons (wet and dry) were higher than the standards recommended by USEPA and WHO. Also, the concentrations of Fe were greater than 25.3 µg m⁻³ (wet season) and 18.3 µg m⁻³ (dry season) reported by Kumar *et al.* (2018). In addition, these values are higher than $31 \times 10^{-3} \mu\text{g m}^{-3}$ given by Antisari *et al.*⁴⁴

Gold (Au) was detected at two sampling spots only in the wet season, SS 6 ($4.849 \times 10^3 \pm 2.396 \times 10^3 \mu\text{g m}^{-3}$) and SS 9 ($4.615 \times 10^3 \pm 2.2843 \times 10^3 \mu\text{g m}^{-3}$). The concentration values of Au were higher than the stipulated values by USEPA and WHO. Au was not detected in the dry season.

Silver (Ag) was characterized in the wet samples with the highest concentration ($23.200 \times 10^3 \pm 3.112 \times 10^3 \mu\text{g m}^{-3}$) at SS 9, while the lowest concentration of ($11.554 \times 10^3 \pm 2.204 \times 10^3 \mu\text{g m}^{-3}$) was observed at SS 2. On the other hand, the concentration ($20.912 \times 10^3 \pm 2.962 \times 10^3 \mu\text{g m}^{-3}$) at SS 9 also gave the highest in the dry season, while the lowest ($10.712 \times 10^3 \pm 2.689 \times 10^3 \mu\text{g m}^{-3}$) was found at SS 5. The concentrations at all locations were higher than the USEPA and WHO set standard of 35 µg m⁻³ and 25 µg m⁻³ respectively.

The highest concentration of palladium (Pd) $16.268 \times 10^3 \pm 2.237 \times 10^3 \mu\text{g m}^{-3}$ in the characterized samples, in the wet season, was observed at SS 4, while the lowest concentration ($11.872 \times 10^3 \pm 1.692 \times 10^3 \mu\text{g m}^{-3}$) was recorded at SS2. Similarly, the highest ($16.090 \times 10^3 \pm 3.132 \times 10^3 \mu\text{g m}^{-3}$) concentration of Pd was obtained at SS 8 in the dry season, while SS 1 has the lowest ($10.055 \times 10^3 \pm 0.991 \times 10^3 \mu\text{g m}^{-3}$). The values obtained in the two seasons were higher than the USEPA and WHO standards.

Rhodium (Rh) was characterized in the wet samples with the highest concentration ($54.136 \times 10^3 \pm 2.712 \times 10^3 \mu\text{g m}^{-3}$) at SS

Table 4 Wet season heavy metal concentration from selected sampling spots^a

Elements	µg m ⁻³ (10 ³)										Control
	SS 1	SS 2	SS 3	SS 4	SS 5	SS 6	SS 7	SS 8	SS 9	SS10	
Fe	72.569	111.650	59.909	54.441	81.104	59.536	77.941	69.061	30.679	58.238	44.631
Au	—	—	—	—	—	4.849	—	—	4.615	—	—
Ag	15.191	11.554	15.195	16.733	16.636	16.645	13.612	18.021	23.200	17.672	14.763
Pd	13.806	11.872	13.222	16.268	13.135	15.091	13.118	14.554	15.113	14.092	12.032
Rh	40.931	34.133	37.080	54.136	36.365	41.810	33.376	39.850	51.084	45.576	38.837
Cd	27.483	19.529	23.694	28.078	19.209	23.890	21.477	25.906	32.407	31.182	22.683
Zn	4.224	6.651	2.321	4.996	7.171	4.072	7.667	6.513	3.128	5.532	1.971
In	23.380	18.550	21.254	29.581	24.070	25.284	17.710	27.051	33.129	30.214	24.920
Sn	25.223	17.107	22.236	24.218	18.836	22.741	15.781	24.830	29.497	21.245	6.368
Cu	4.292	—	—	—	—	—	—	8.456	—	6.115	—
Mn	—	—	—	6.111	—	—	4.692	—	—	4.591	—
Ti	59.967	39.830	77.145	61.716	57.692	66.638	61.716	56.232	81.337	68.712	30.264
Ru	7.618	5.887	6.287	9.127	6.617	7.552	5.705	7.911	8.987	11.168	6.728

^a SS: sampling spot.



Table 5 Dry season heavy metal concentration from selected sampling spots^a

Elements	$\mu\text{g m}^{-3} (10^3)$										Control
	SS 1	SS 2	SS 3	SS 4	SS 5	SS 6	SS 7	SS 8	SS 9	SS 10	
Fe	65.216	117.369	64.907	58.841	75.845	66.117	74.814	78.882	71.591	64.873	40.775
Ag	14.816	14.256	14.600	13.793	10.712	13.141	15.124	17.355	20.912	16.879	5.779
Pd	10.055	10.950	10.548	10.336	13.027	12.984	13.966	16.090	12.858	13.546	4.257
Rh	39.296	40.073	49.705	50.420	43.516	43.390	42.053	40.784	41.675	47.632	23.215
Cd	30.775	36.293	31.515	38.002	34.670	35.813	33.801	29.326	34.528	40.658	16.512
Zn	7.383	7.062	7.972	7.569	8.256	7.113	7.147	8.439	9.575	9.060	4.076
In	30.951	31.533	32.937	33.979	39.602	35.213	39.011	39.964	37.513	36.509	14.767
Sn	30.449	28.356	28.885	32.747	33.616	34.408	35.851	33.131	38.872	36.832	23.892
W	—	39.939	—	—	—	—	—	45.297	—	—	—
Cu	4.799	—	—	7.552	—	4.987	—	8.456	7.351	—	—
Ti	66.240	59.111	85.865	79.968	74.118	50.451	44.101	82.033	66.369	59.150	38.833
Ru	10.644	8.711	7.989	10.640	7.425	9.737	11.510	8.323	10.376	10.764	3.780
S	9.903	8.922	—	—	9.555	—	7.871	—	8.141	7.539	—

^a SS: sampling spot.

4, while the lowest concentration of $(33.376 \times 10^3 \pm 1.959 \times 10^3 \mu\text{g m}^{-3})$ was observed at SS 7. On the other hand, the concentration $(50.420 \times 10^3 \pm 1.303 \times 10^3 \mu\text{g m}^{-3})$ at SS 4 also gave the highest in the dry season, while the lowest $(39.296 \times 10^3 \pm 2.821 \times 10^3 \mu\text{g m}^{-3})$ was found at SS 1. The concentrations at all locations were higher than the USEPA and WHO set standards of $35 \mu\text{g m}^{-3}$ and $25 \mu\text{g m}^{-3}$, respectively.

The highest concentration $(32.407 \times 10^3 \pm 4.160 \times 10^3 \mu\text{g m}^{-3})$ of cadmium (Cd) characterized in the wet samples was collected at SS 9, while the lowest $(19.209 \times 10^3 \pm 3.419 \times 10^3 \mu\text{g m}^{-3})$ was found in the samples collected at SS 5. Analysis of particulates deposited in the dry season indicated the highest concentration $(40.658 \times 10^3 \pm 2.441 \times 10^3 \mu\text{g m}^{-3})$ at SS 10, while the lowest $(29.321 \times 10^3 \pm 2.770 \times 10^3 \mu\text{g m}^{-3})$ was recorded at SS 8. These values were higher than the USEPA and WHO standards. They were all higher than $(1 \times 10^{-2} \mu\text{g m}^{-3})$ wet season and $(3.9 \times 10^{-2} \mu\text{g m}^{-3})$ dry season values reported by Kumar *et al.* (2018), as well as $0.5 \times 10^{-2} \mu\text{g m}^{-3}$ (ref. 44) and $9.18 \mu\text{g m}^{-3}$.³³

Zinc (Zn) recorded the highest concentration $(7.667 \times 10^3 \pm 1.067 \times 10^3 \mu\text{g m}^{-3})$ in the wet season at SS 7, while the lowest concentration $(2.321 \times 10^3 \pm 0.849 \times 10^3 \mu\text{g m}^{-3})$ was detected at SS 3. The highest concentration $(9.575 \times 10^3 \pm 1.411 \times 10^3 \mu\text{g m}^{-3})$ was found at SS 9 in the dry season, while the lowest $(7.062 \times 10^3 \pm 1.624 \times 10^3 \mu\text{g m}^{-3})$ was recorded at SS 2. The concentrations at all locations in the wet and dry seasons were higher than the USEPA and WHO standards. They were also higher than $(0.941 \mu\text{g m}^{-3})$ wet season and $(2.48 \mu\text{g m}^{-3})$ dry season values by Kumar *et al.*⁴³ and $22.2 \times 10^{-3} \mu\text{g m}^{-3}$ reported by Antisari *et al.*⁴⁴

The highest concentration $(33.129 \times 10^3 \pm 5.168 \times 10^3 \mu\text{g m}^{-3})$ for indium (In) was observed in the wet samples at SS 9, while the lowest $(17.710 \times 10^3 \pm 2.807 \times 10^3 \mu\text{g m}^{-3})$ was recorded at SS 7. The highest concentration $(39.964 \times 10^3 \pm 2.347 \times 10^3 \mu\text{g m}^{-3})$ in the dry season was observed at SS 8, while the lowest $(30.951 \times 10^3 \pm 3.511 \times 10^3 \mu\text{g m}^{-3})$ was recorded at SS 1. All the characterized concentrations were

higher than the recommended USEPA ($35 \mu\text{g m}^{-3}$) and WHO ($25 \mu\text{g m}^{-3}$) standards.

Tin (Sn) was detected in the characterized samples collected for both seasons. The highest concentration $(29.497 \times 10^3 \pm 6.353 \times 10^3 \mu\text{g m}^{-3})$ was recorded at SS 9, while the lowest concentration $(15.781 \times 10^3 \pm 3.473 \times 10^3 \mu\text{g m}^{-3})$ was recorded at SS 7 in the wet season. The highest concentration $(38.872 \times 10^3 \pm 6.853 \times 10^3 \mu\text{g m}^{-3})$ in the dry season was also recorded at SS 9, while the lowest concentration $(28.356 \times 10^3 \pm 5.814 \times 10^3 \mu\text{g m}^{-3})$ was found at SS 2 in the dry season. The concentrations at all SS in the wet and dry seasons were higher than USEPA and WHO standards. Their concentrations were equally higher than $(4.1 \times 10^{-2} \mu\text{g m}^{-3})$ wet season and $(14.8 \times 10^{-2} \mu\text{g m}^{-3})$ dry season values given by Kumar *et al.*⁴³

In the dry season, tungsten (W) was detected at two sampling spots, SS 2 ($39.939 \times 10^3 \pm 1.412 \times 10^3 \mu\text{g m}^{-3}$) and SS 8 ($45.297 \times 10^3 \pm 4.634 \times 10^3 \mu\text{g m}^{-3}$). The concentration values of W were higher than the stipulated values by USEPA and WHO. Tungsten was not detected in the wet season.

The highest concentration $(8.456 \times 10^3 \pm 1.763 \times 10^3 \mu\text{g m}^{-3})$ of copper (Cu) was found at SS 8, while the lowest $(4.292 \times 10^3 \pm 2.103 \times 10^3 \mu\text{g m}^{-3})$ was recorded at SS 1 in the wet season. The highest of the dry season characterized concentration $(7.552 \times 10^3 \pm 2.307 \times 10^3 \mu\text{g m}^{-3})$ was found at SS 4, while the lowest concentration $(4.799 \times 10^3 \pm 2.040 \times 10^3 \mu\text{g m}^{-3})$ was also recorded at SS 1. The values were higher than the stipulated USEPA ($35 \mu\text{g m}^{-3}$) and WHO ($25 \mu\text{g m}^{-3}$) standards. The characterized concentrations of Cu were also higher than $(16.9 \times 10^{-2} \mu\text{g m}^{-3})$ wet season and $(49.4 \times 10^{-2} \mu\text{g m}^{-3})$ dry season values reported by Kumar *et al.*,⁴³ as well as $(21.3 \times 10^{-3} \mu\text{g m}^{-3})$ by Antisari *et al.*⁴⁴

The highest concentration of manganese (Mn) $(6.111 \times 10^3 \pm 2.433 \times 10^3 \mu\text{g m}^{-3})$ was detected at SS 4 in the wet season while the lowest concentration $(4.591 \times 10^3 \pm 1.776 \times 10^3 \mu\text{g m}^{-3})$ was found at SS 10. The concentration values were higher than the recommended standards by USEPA and WHO, and they are also much higher than $(28.6 \times 10^{-3} \mu\text{g m}^{-3})$ that



reported by Antisari *et al.*⁴⁴ Manganese was not detected in the dry season.

The highest concentration ($81.337 \times 10^3 \pm 9.861 \times 10^3 \mu\text{g m}^{-3}$) of titanium (Ti) was found at SS 9, while the lowest ($39.830 \times 10^3 \pm 4.759 \times 10^3 \mu\text{g m}^{-3}$) was recorded at SS 2 in the wet season. The highest of the dry season characterized concentration ($85.865 \times 10^3 \pm 6.698 \times 10^3 \mu\text{g m}^{-3}$) was found at SS 3, while the lowest concentration ($44.101 \times 10^3 \pm 6.512 \times 10^3 \mu\text{g m}^{-3}$) was also recorded at SS 7. The values were higher than the stipulated USEPA ($35 \mu\text{g m}^{-3}$) and WHO ($25 \mu\text{g m}^{-3}$) standards.

Ruthenium (Ru) was detected in the characterized samples. The concentration ($11.168 \times 10^3 \pm 0.787 \times 10^3 \mu\text{g m}^{-3}$) was highest at SS 10, while the lowest concentration ($5.705 \times 10^3 \pm 0.577 \times 10^3 \mu\text{g m}^{-3}$) was found at SS 7 in the wet season. The dry season analysis shows that the highest concentration ($11.510 \times 10^3 \pm 1.278 \times 10^3 \mu\text{g m}^{-3}$) was found at SS 7, while the lowest concentration ($7.425 \times 10^3 \pm 1.690 \times 10^3 \mu\text{g m}^{-3}$) was found at SS 5. The characterized results for ruthenium were higher in concentration when compared with the standard values by USEPA and WHO.

The concentration ($9.903 \times 10^3 \pm 0.694 \times 10^3 \mu\text{g m}^{-3}$) of sulphur (S) in the characterized dry samples was highest at SS 1, while the lowest concentration ($7.539 \times 10^3 \pm 0.933 \times 10^3 \mu\text{g m}^{-3}$) was found at SS 10. The concentration values were higher than the stipulated values by USEPA and WHO. Sulphur was not detected in the wet season. In the wet season, Fe had the highest concentration of $72.569 \times 10^3 \mu\text{g m}^{-3}$ in SS 1, while Zn had the lowest concentration of $4.224 \times 10^3 \mu\text{g m}^{-3}$; the metal concentrations were in the following order Fe > Ti > Rh > Cd > Sn > In > Ag > Pd > Ru > Cu > Zn. In the dry season, Ti had the highest concentration of $66.24 \times 10^3 \mu\text{g m}^{-3}$ in SS 1, while Cu had the lowest concentration of $4.799 \times 10^3 \mu\text{g m}^{-3}$; the metal concentrations followed the order as Ti > Fe > Rh > In > Cd > Sn > Ag > Ru > Pd > S > Zn > Cu. Fe also had the highest concentration of $111.65 \times 10^3 \mu\text{g m}^{-3}$ and $117.369 \times 10^3 \mu\text{g m}^{-3}$ in the wet and dry seasons respectively at SS 2, while Ru had the lowest concentration of $5.887 \times 10^3 \mu\text{g m}^{-3}$ in the wet season, also Zn had the lowest concentration of $7.062 \times 10^3 \mu\text{g m}^{-3}$ in the dry season.

The trend of the metal concentration Fe > Ti > Rh > Cd > In > Sn > Pd > Ag > Zn > Ru was observed in the wet season, while the concentration of metals was in the order Fe > Ti > Rh > W > Cd > In > Sn > Ag > Pd > S > Ru > Zn.

In the wet season, from SS 3 and SS 4 respectively, Ti had the highest concentration of $77.145 \times 10^3 \mu\text{g m}^{-3}$ and $61.716 \times 10^3 \mu\text{g m}^{-3}$ while Zn had the lowest concentration of $2.321 \times 10^3 \mu\text{g m}^{-3}$ and $4.996 \times 10^3 \mu\text{g m}^{-3}$ with the following order Ti > Fe > Rh > Cd > Sn > In > Ag > Pd > Ru > Zn and Ti > Fe > Rh > In > Cd > Sn > Ag > Pd > Ru > Mn > Zn respectively from SS 3 and SS 4. In the dry season, from SS 3 and SS 4 respectively, Ti also had the highest concentration of $85.865 \times 10^3 \mu\text{g m}^{-3}$ and $79.968 \times 10^3 \mu\text{g m}^{-3}$ while Zn and Cu had the lowest concentration of $7.972 \times 10^3 \mu\text{g m}^{-3}$ and $7.552 \times 10^3 \mu\text{g m}^{-3}$; the metal concentration followed the order as Ti > Fe > Rh > In > Cd > Sn > Ag > Pd > Ru > Zn and Ti > Fe > Rh > Cd > In > Sn > Ag > Ru > Pd > Zn > Cu at SS 3 and SS 4 respectively.

Fe had the highest concentration of $81.104 \times 10^3 \mu\text{g m}^{-3}$ in the wet season at SS 5, while Ru had the lowest concentration of $6.617 \times 10^3 \mu\text{g m}^{-3}$ in the following order Fe > Ti > Rh > In > Cd > Sn > Ag > Pd > Zn > Ru. Similarly in the dry season, Fe had the highest concentration of $75.845 \times 10^3 \mu\text{g m}^{-3}$ at SS 5, while Ru also had the lowest concentration of $7.425 \times 10^3 \mu\text{g m}^{-3}$; the concentration of metals was in the order Fe > Ti > Rh > In > Cd > Sn > Pd > Ag > S > Zn > Ru. In SS 6, Ti had the highest concentration of $66.638 \times 10^3 \mu\text{g m}^{-3}$ in the wet season, with Zn having the lowest concentration of $4.072 \times 10^3 \mu\text{g m}^{-3}$ in the following order Ti > Fe > Rh > In > Cd > Sn > Ag > Pd > Ru > Au > Zn. In the dry season, the concentration of Fe was the highest with $66.117 \times 10^3 \mu\text{g m}^{-3}$ with Cu having the lowest concentration of $4.799 \times 10^3 \mu\text{g m}^{-3}$ in the following order Fe > Ti > Rh > Cd > In > Sn > Ag > Pd > Ru > Zn > Cu. In the wet season, Fe had the highest concentration at both SS 7 and SS 8 with $77.941 \times 10^3 \mu\text{g m}^{-3}$ and $69.061 \times 10^3 \mu\text{g m}^{-3}$; the metal concentration followed the order as Fe > Ti > Rh > Cd > In > Sn > Ag > Pd > Zn > Ru > Mn and Fe > Ti > Rh > In > Cd > Sn > Ag > Pd > Cu > Ru > Zn respectively.

Meanwhile in the dry season, Fe also had the highest concentration of $74.814 \times 10^3 \mu\text{g m}^{-3}$ at SS 7 while the concentration of Zn was the lowest with $7.147 \times 10^3 \mu\text{g m}^{-3}$ in the following order Fe > Ti > Rh > In > Sn > Cd > Ag > Pd > Ru > S > Zn. At SS 8, Ti had the highest concentration of $78.882 \times 10^3 \mu\text{g m}^{-3}$ while Ru had the lowest concentration of $8.323 \times 10^3 \mu\text{g m}^{-3}$; the metal concentration followed the order Ti > Fe > W > Rh > In > Sn > Cd > Ag > Pd > Zn > Ru.

At SS 9 and SS 10, in the wet season, Ti had the highest concentration of $81.337 \times 10^3 \mu\text{g m}^{-3}$ and $68.712 \times 10^3 \mu\text{g m}^{-3}$ respectively. The concentration of Zn was the lowest $3.128 \times 10^3 \mu\text{g m}^{-3}$ at SS 9, and Mn also had the lowest concentration of $4.591 \times 10^3 \mu\text{g m}^{-3}$ at SS 10. The metal concentration followed the order as Ti > Rh > In > Cd > Fe > Sn > Ag > Pd > Ru > Au > Zn and Ti > Fe > Rh > Cd > In > Sn > Ag > Pd > Ru > Cu > Zn > Mn at SS 9 and SS 10, respectively. In the dry season at SS 9 and SS 10, Fe had the highest concentration of $71.591 \times 10^3 \mu\text{g m}^{-3}$ and

Table 6 Deposition fluxes at selected sampling spots^a

SS	Wet season		Dry season	
	(g per m ² per month)	(g m ⁻² s ⁻¹) 10 ⁻⁶	(g per m ² per month)	(g m ⁻² s ⁻¹) 10 ⁻⁵
1	9.55	3.68	41.37	1.60
2	10.82	4.17	48.7	1.88
3	8.59	3.31	38.83	1.50
4	11.46	4.42	64.61	2.50
5	7.32	2.82	60.47	2.33
6	10.18	3.93	71.93	2.78
7	7.96	3.07	52.51	2.03
8	9.87	3.81	42.97	1.66
9	9.23	3.56	88.80	3.43
10	7.64	2.95	79.89	3.08
Control	0.95	0.37	33.74	1.30

^a Average flux in the wet season = 3.57×10^{-6} (g m⁻² s⁻¹). Average flux in the dry season = 2.28×10^{-5} (g m⁻² s⁻¹).



Table 7 Deposition velocities of trace metals (m s^{-1}) in wet and dry seasons

Trace metals	Trace metal concentration in ppt ($\mu\text{g m}^{-3}$)	Deposition velocity (m s^{-1})	
		Wet season	Dry season
Fe	67 512.8	0.00005288	0.0003377
Au	4732	0.00075444	0.0048183
Ag	16 445.9	0.00021708	0.0013864
Pd	14 027.1	0.00025451	0.0016254
Rh	41 434.1	0.00008616	0.0005503
Cd	25 285.5	0.00014119	0.0009017
Zn	5227.5	0.00068293	0.0043615
In	25 032.3	0.00014262	0.0009108
Sn	22 171.4	0.00016102	0.0010284
Cu	6287.7	0.00056778	0.0036261
Mn	5131.3	0.00069573	0.0044433
Ti	63 098.5	0.00005658	0.0003613
Ru	7685.9	0.00046449	0.0029665

Table 8 Range of deposition velocities (m s^{-1}) from previous studies

Authors	Year	Range
Mamun <i>et al.</i>	2022	0.081–0.112
Yan <i>et al.</i>	2014	0.0019–0.0817
Zhang <i>et al.</i>	2012	0.0015–0.0331
Qi <i>et al.</i>	2005	0.008–1
Lestari <i>et al.</i>	2003	0.0021–0.893
Yun <i>et al.</i>	2002	0.0011–0.004

$64.873 \times 10^3 \mu\text{g m}^{-3}$. The metal concentration followed the order $\text{Fe} > \text{Ti} > \text{Rh} > \text{Sn} > \text{In} > \text{Cd} > \text{Ag} > \text{Pd} > \text{Ru} > \text{Zn} > \text{S} > \text{Cu}$ and $\text{Fe} > \text{Ti} > \text{Rh} > \text{Cd} > \text{Sn} > \text{In} > \text{Ag} > \text{Pd} > \text{Ru} > \text{Zn} > \text{S}$, respectively. The concentration of Cu was the lowest ($7.351 \times 10^3 \mu\text{g m}^{-3}$) at SS 9, while S had the lowest concentration of $7.539 \times 10^3 \mu\text{g m}^{-3}$ at SS 10.

As discussed in this section, all the heavy metals characterized are exponentially higher than the stipulated standard. The

result obtained showed that heavy metals are being released through the open burning of solid wastes, and the emission has a significant influence on the concentration of the heavy metals in the particulate samples collected, which is in accordance with Kumar *et al.*,⁴³ and combustion of solid waste releases high number of particulates and metals into the environment. Some of these heavy metals trigger human poisoning (acute/chronic) after being exposed through food or air. Their accumulation in the human body causes harmful effects on organs and tissues, such as deoxyribonucleic acid (DNA) and membrane damage, neurotoxicity, skin toxicity, cancer, cardio-vascular toxicity among others.^{45,46} Globally, heavy metal contamination is gradually turning into a critical issue of concern as a result of the release of air emissions from human activities such as open burning of solid waste.^{47,48}

3.2.3 Deposition velocities and scavenging ratios. The deposition velocities of the heavy metals were evaluated as the flux per concentration of the heavy metals precipitated. The evaluated deposition flux ($\text{g m}^{-2} \text{s}^{-1}$) and deposition velocity (m s^{-1}) are presented in Tables 6 and 7, respectively. In the wet season, Au had the highest deposition velocity of $0.00075444 \text{ m s}^{-1}$ while Fe had the lowest ($0.0000528 \text{ m s}^{-1}$). In the dry season, Au also had the highest deposition velocity of $0.0048183 \text{ m s}^{-1}$ while Fe also had the lowest velocity of $0.0003377 \text{ m s}^{-1}$. Owing to the higher deposition velocity of Au, its lifetime in the particles of the study area is governed by dry deposition, whereas that of Fe is governed by wet deposition. As a result, the scavenging ratio is a better parameter to use for Fe to parametrize its removal mechanism in the atmosphere. The range of deposition velocities from previous studies is shown in Table 8.

The results of the scavenging ratio in the wet season (Table 9) revealed that Cu, Ti, Mn and Fe had the highest scavenging ratios, which were estimated to be 3.96, 3.39, 1.89 and 1.46 respectively. Meanwhile Zn, Ag, Sn and Cd were characterized with lower scavenging ratios of 0.66, 0.74, 0.77 and 0.95 respectively. Also, in the dry season, the scavenging ratio (Table 10) shows that Cu, Ti, Fe and In had the highest scavenging ratios, which were estimated to be 2.1, 1.57, 1.57 and 1.12

Table 9 Scavenging ratios of trace metals in the wet season

Trace metals	Trace metal concentration in air (6 hours) ($\mu\text{g m}^{-3}$)	Trace metal concentration in ppt (720 hours) ($\mu\text{g m}^{-3}$)	Scavenging ratio
Fe	46 208	67 512.8	1.46
Au	5107	4732	0.93
Ag	22 228	16 445.9	0.74
Pd	14 643	14 027.1	0.96
Rh	38 794	41 434.1	1.07
Cd	26 605	25 285.5	0.95
Zn	7980	5227.5	0.66
In	26 531	25 032.3	0.94
Sn	28 790	22 171.4	0.77
Cu	1588	6287.7	3.96
Mn	2746	5131.3	1.89
Ti	18 672	63 098.5	3.39
Ru	7190	7685.9	1.07



Table 10 Scavenging ratios of trace metals in the dry season

Trace metals	Trace metal concentration in air (6 hours) ($\mu\text{g m}^{-3}$)	Trace metal concentration in ppt (720 hours) ($\mu\text{g m}^{-3}$)	Scavenging ratio
Fe	47 097	73 845.5	1.57
Au	8440	—	—
Ag	24 793	15 158.8	0.61
Pd	16 544	12 436	0.75
Rh	44 620	43 854.4	0.98
Cd	32 443	34 538.1	1.06
Zn	9648	7957.6	0.82
In	31 955	35 721.2	1.12
Sn	35 998	33 314.7	0.93
W	—	42 618	—
Cu	2946	6172.3	2.10
Mn	3932	—	—
Ti	42 641	66 740.6	1.57

respectively. However, Ag, Pd, Zn and Ru were characterized with lower scavenging ratios of 0.61, 0.75, 0.82 and 0.89 respectively. As a result, Cu, Ti, Mn, and Fe may be better removed in the atmosphere near solid waste combustion sites *via* wet deposition. Wet deposition may influence the lifetime of Cu, Ti, Mn, and Fe in the environment, whereas dry deposition governs the lifetime of Zn, Ag, Sn, Au, and Cd. The contribution of scavenging particulate trace metals to the deposition flux was calculated using trace metal scavenging ratios, which are the concentrations of trace metals in precipitation divided by their concentrations in air.

In this study, the estimated value of the highest deposition velocity was found to be that of Au ($0.0048183 \text{ m s}^{-1}$) which is lower than the values reported by Yan *et al.*,⁴⁹ Zhang *et al.*⁵⁰ and Qi *et al.*⁵¹ but higher than the result of Jimoda *et al.*³³ The lowest value corresponds to that of Fe ($0.0003377 \text{ m s}^{-1}$) which is lower to those reported by previous studies.^{49,51,52} The highest deposition velocity from trace metals in the Sokoto Aiyekale dump site, Ilorin was found to be almost the same when compared with the work of Yun *et al.*,⁵³ which obtained a deposition velocity of 0.004 m s^{-1} . The estimated scavenging ratio for the trace metals in the government approved dump site, Ilorin was in the range 0.61–3.96, which is comparable to the one estimated by Alamu *et al.*⁵⁴ A series of reviewed literature studies showed that there is paucity of information on dispersion modelling of pollutants from open burning of municipal solid waste. Researchers like Adeniran *et al.*,⁵⁵ Ipeaiyeda and Falusi,⁵⁶ Fakinle *et al.*,⁵⁷ Daffi *et al.*⁵⁸ and Pansuk *et al.*⁵⁹ assessed the air pollution from household and local open burning of solid wastes in dump sites along the road/across the streets using handheld gas analyzers without modelling the gases to evaluate the dynamics of the pollutants as they travel to receptor communities. Meanwhile, this study considered Ilorin as a state capital (with over 1 million population), which is the only state capital in Nigeria with one government approved dumpsite in the city. Thus, with the magnitude of waste being burned daily on a 600 plot (390 000 sqm) Sokoto-Aiyekale dump site in Ilorin metropolis with 130 burning points, the receptor communities, workers and the environment could be at risk of release of

hazardous cocktail of emissions. There is hence the need for forward trajectory modelling with an American Meteorological Society/Environmental Protection Agency Regulatory Model (AERMOD) dispersion model to assess and evaluate the impact on air quality in the receptor communities surrounding the Sokoto-Aiyekale dump site.

3.3 Dispersion modelling study

The ISC-AERMORD modelling outputs of ground level concentrations for PM and VOC emissions during the study are herein presented in this section. These are guided by the available averaging period standards of the modelled air pollutants. Impacts of the open burning of solid waste on ambient air quality are also discussed. The emission sources obtained in the study having estimated to the appropriate unit before inputting them into the dispersion protocol are estimated in Table 11.

3.3.1 The receptor locations. The communities identified and considered as receptors to air pollutants by open burning of solid waste on the Sokoto-Aiyekale dump site include Sokoto, Abe Emi, Ayekale, Wara, Airport, Olorunsogo, Osere, Oko-Erin, Asa Dam, Orisumibare, and Egbejila. All these were found to be within the designated kilometer locations shown in Fig. 1.

3.3.2 Predicted ground level concentration of CAPs. The modelling outputs of ground level concentrations for all the CAPs as obtained during the study are herein presented.

3.3.2.1 PM emissions around the receptor locations. The 1 h predicted concentrations of particulate matter have values in the range $7882\text{--}788\,220 \mu\text{g m}^{-3}$ as shown in Fig. 3. The 8 h

Table 11 Total average emissions (g s^{-1})

Year	PM	VOCs
2016	69.8	187.5
2017	72.0	193.3
2018	74.1	199.1
2019	76.4	205.2
2020	78.7	211.4
Average	74.2	199.3



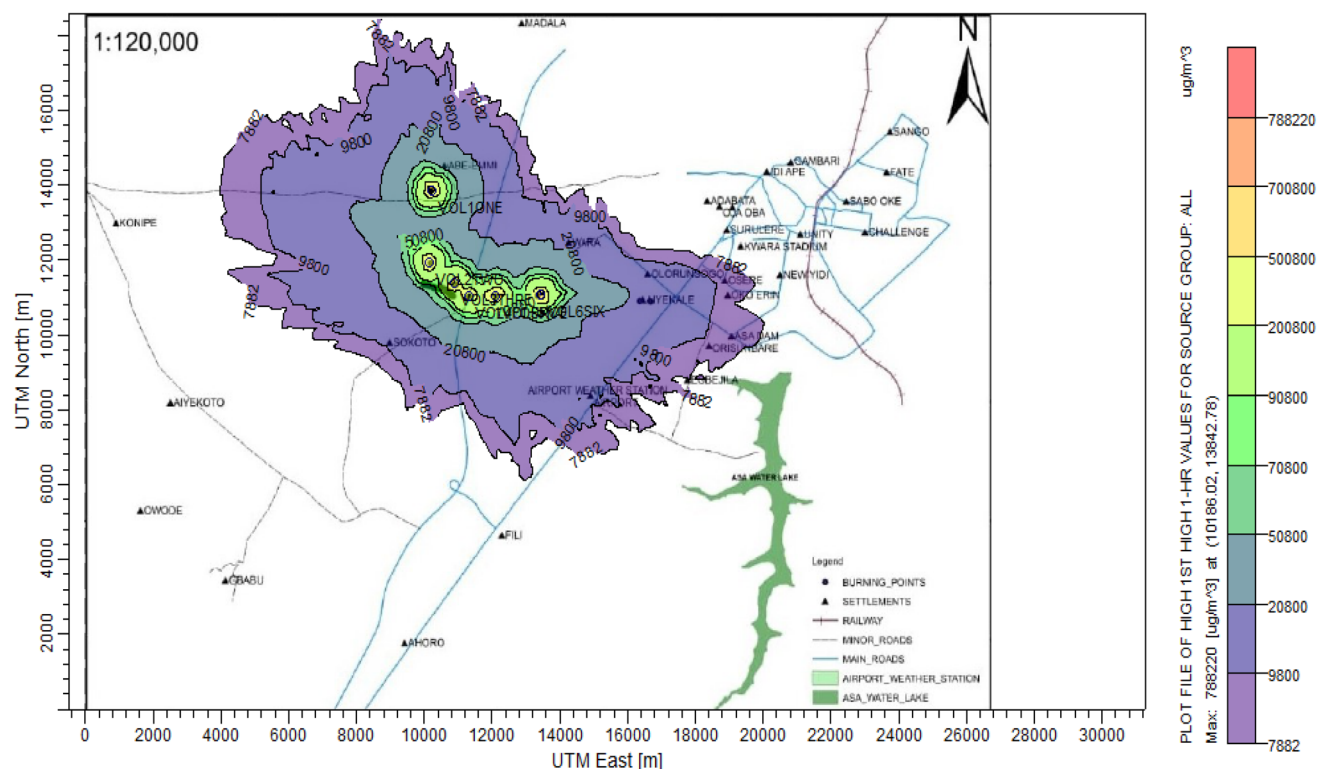


Fig. 3 1 hour ground level PM isopleth from the Sokoto-Aiyekale dump site.

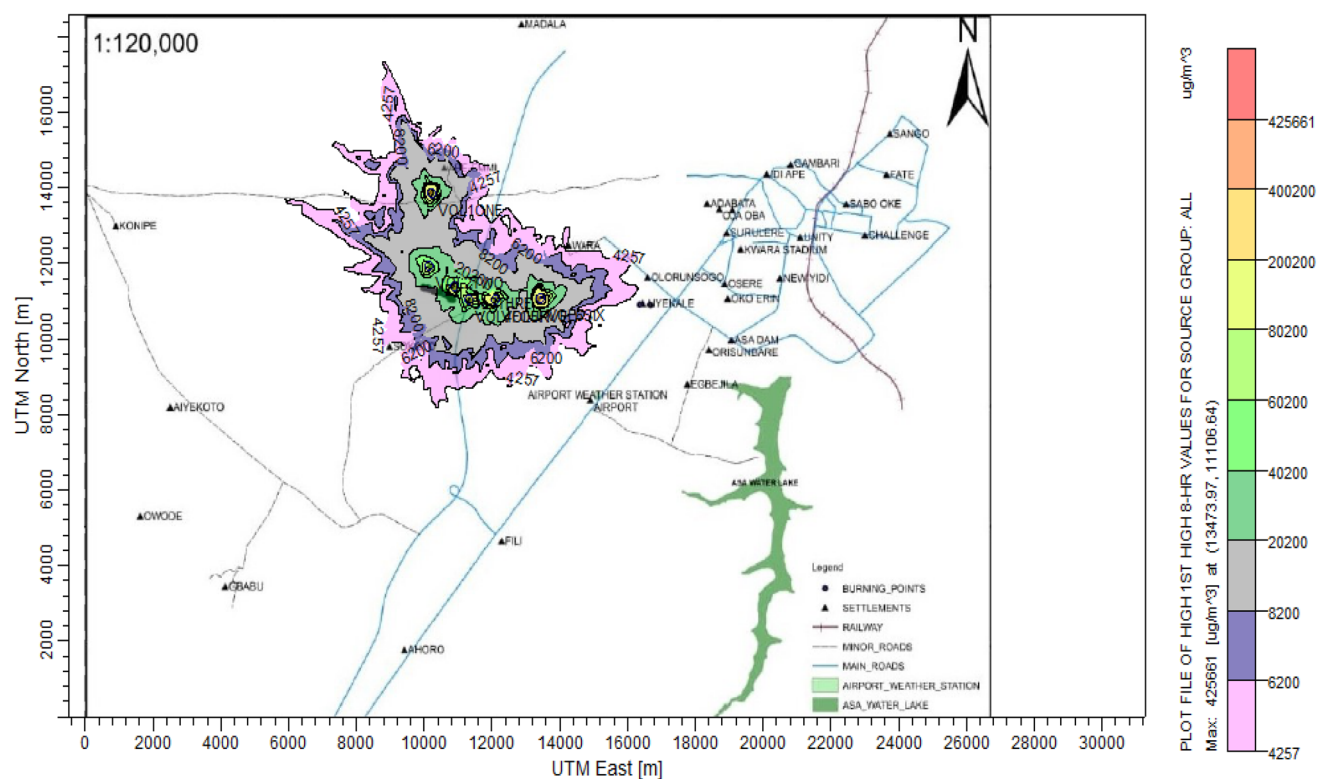


Fig. 4 8 hour ground level PM isopleth from the Sokoto-Aiyekale dump site.

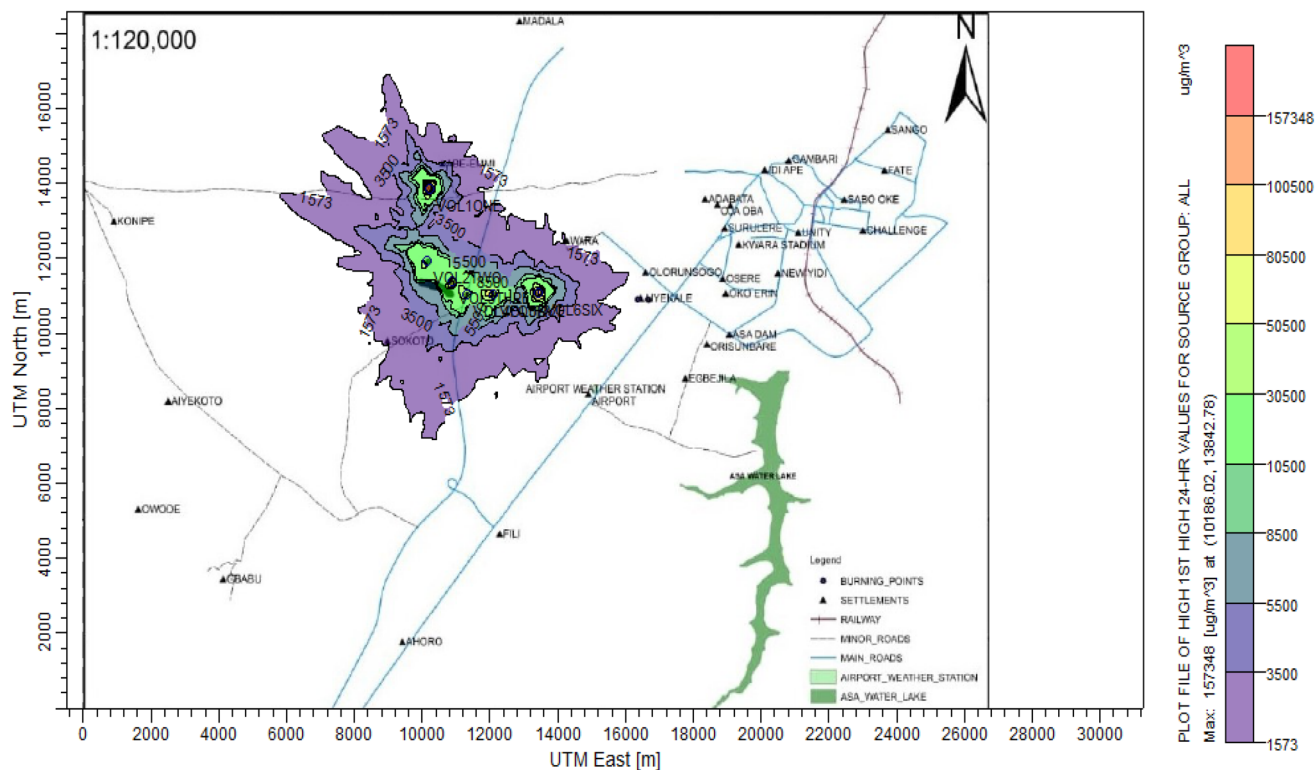


Fig. 5 24 hour ground level PM isopleth from the Sokoto-Aiyekale dump site.

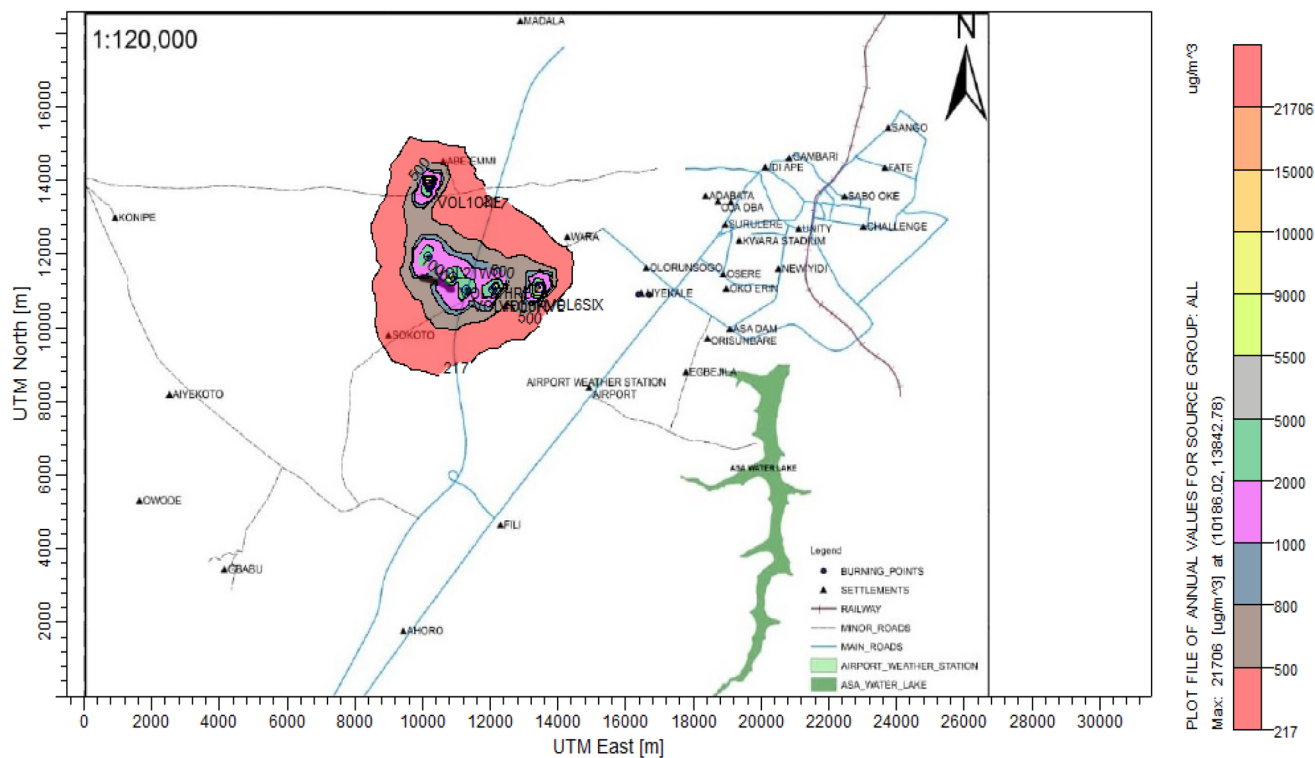


Fig. 6 Annual ground level PM isopleth from the Sokoto-Aiyekale dump site.



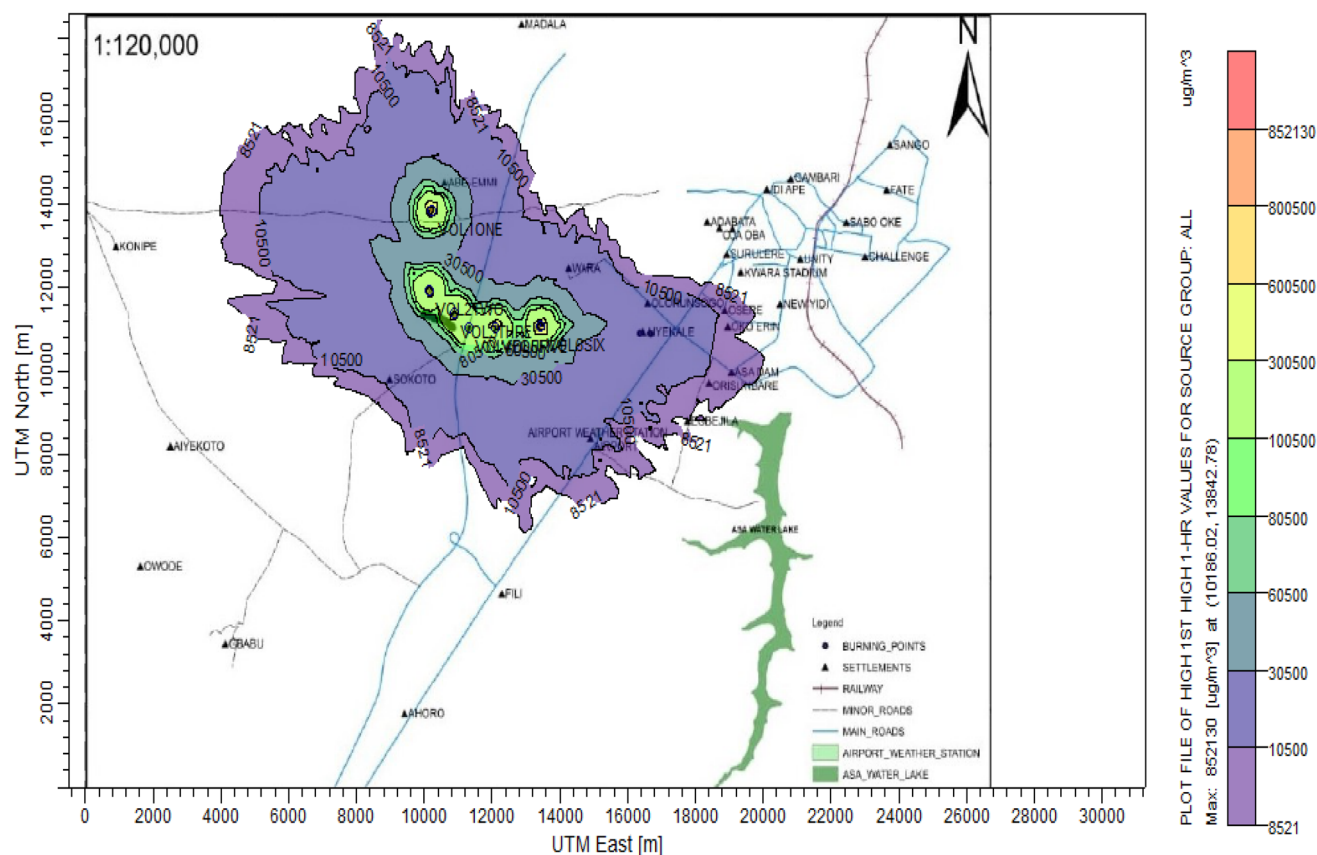


Fig. 7 1 hour ground level VOC isopleth from the Sokoto-Aiyekale dump site.

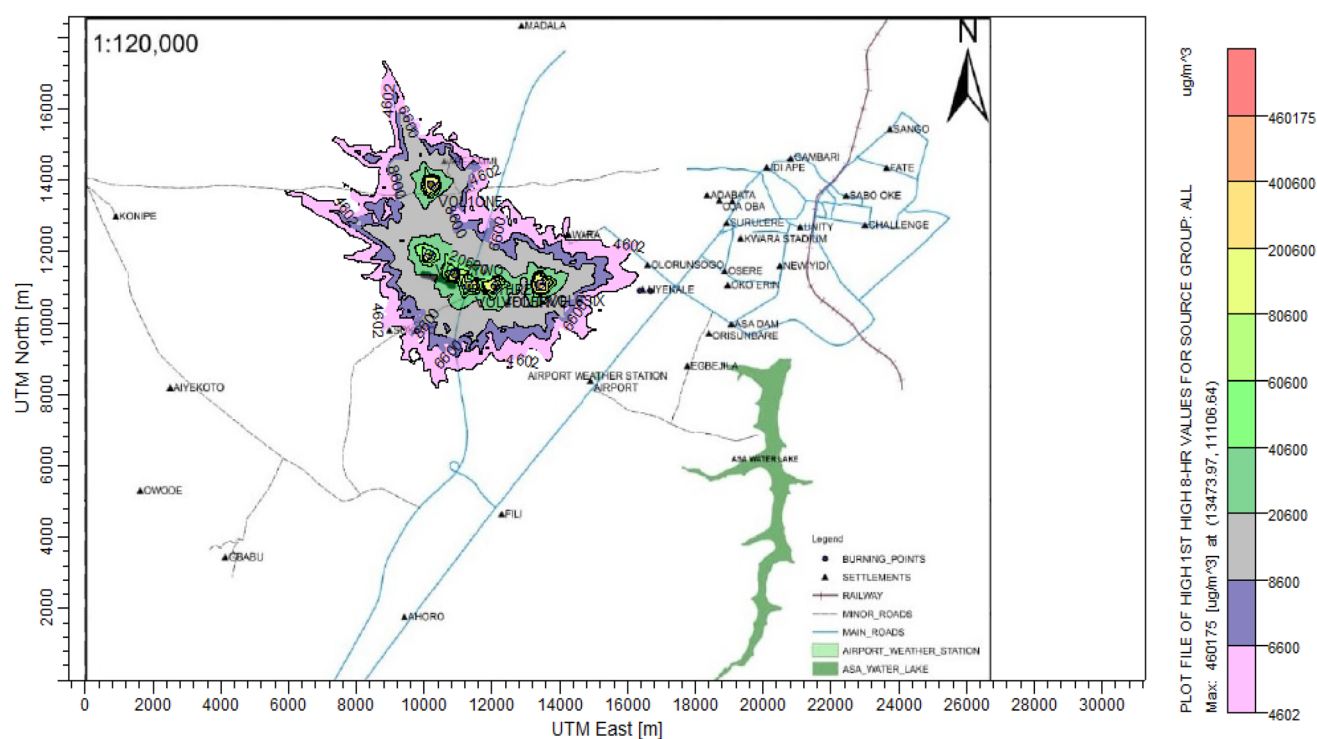


Fig. 8 8 hour ground level VOC isopleth from the Sokoto-Aiyekale dump site.

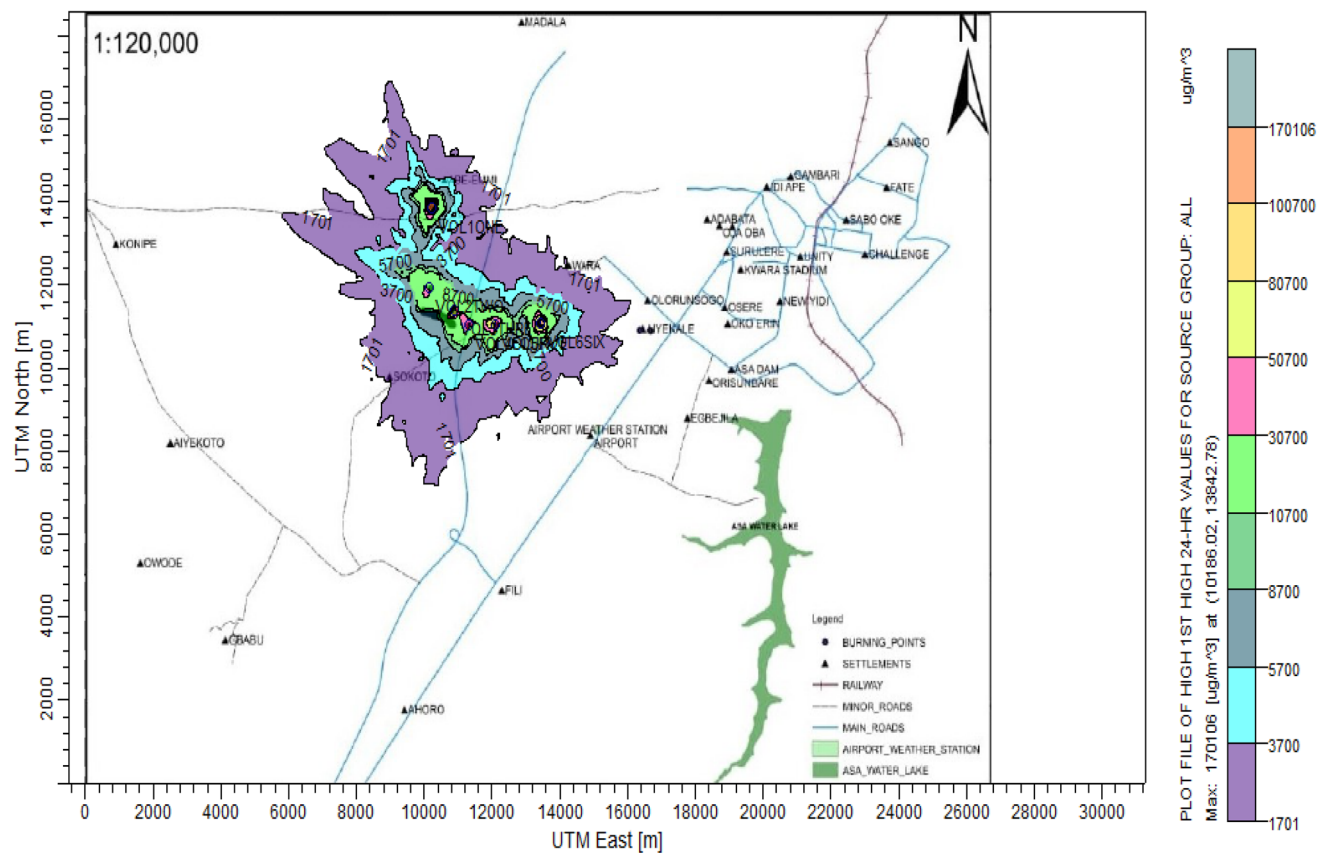


Fig. 9 24 hour ground level VOC isopleth from the Sokoto-Aiyekale dump site.

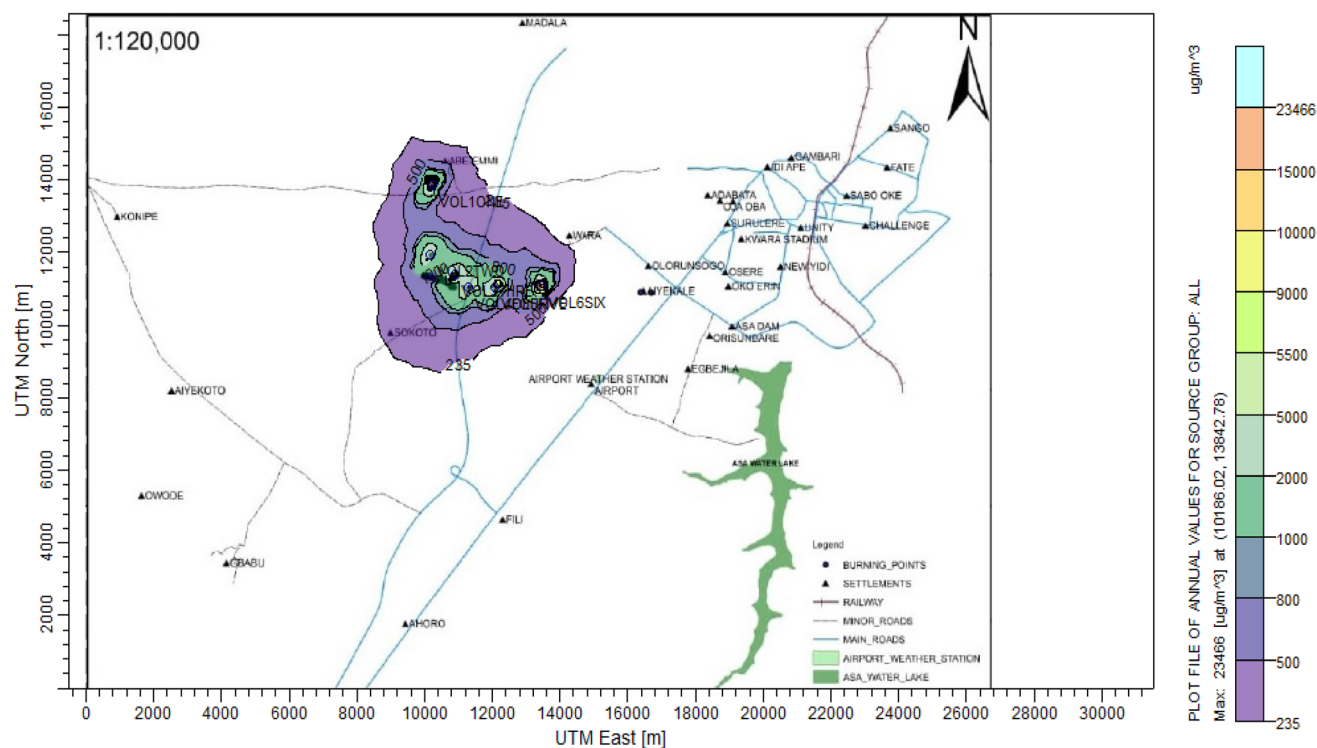


Fig. 10 Annual ground level VOC isopleth from the Sokoto-Aiyekale dump site.



Table 12 Predicted PM cumulative impacts around the Sokoto-Aiyekale dump site

Receptor	Predicted concentration ($\mu\text{g m}^{-3}$)				% Recommended in FMEnV		% Recommended limit in WHO
	1 h	8 h	24 h	Annual	1 h (600 $\mu\text{g m}^{-3}$)	24 h (150 $\mu\text{g m}^{-3}$)	Annual (40–60 $\mu\text{g m}^{-3}$)
Sokoto	15 300	5229	2537	359	25.50	16.91	8.98
Aiyekale	15 300	4257	—	—	25.50	—	—
Abe-Emi	50 800	14 200	4500	650	84.67	30	16.25
Wara	20 800	5229	2537	217	34.67	16.91	5.43
Airport	15 300	—	—	—	25.50	—	—
Olorunsogo	15 300	4257	—	—	25.50	—	—
Osere	9800	—	—	—	16.33	—	—
Oko Erin	8841	—	—	—	14.74	—	—
Asa-Dam	8841	—	—	—	14.74	—	—
Egbejila	8841	—	—	—	14.74	—	—
Orisumibare	9800	—	—	—	16.33	—	—

predicted concentrations are in the range 4257–425 661 $\mu\text{g m}^{-3}$ as shown in Fig. 4. The 24 h predicted concentrations have values in the range 1573–157 348 $\mu\text{g m}^{-3}$ as shown in Fig. 5. Fig. 6 depicts the annual predicted concentrations, which range from 217 to 21 706 $\mu\text{g m}^{-3}$. The maximum concentrations of particulate matter in the 1 h, 8 h, 24 h and annual averaging periods are 788 220 $\mu\text{g m}^{-3}$, 425 661 $\mu\text{g m}^{-3}$, 157 348 $\mu\text{g m}^{-3}$ and 21 706 $\mu\text{g m}^{-3}$ respectively.

3.3.2.2 VOC emissions around the receptor locations. The 1 h predicted concentrations of VOCs have values in the range 8521–852130 $\mu\text{g m}^{-3}$ as shown in Fig. 7. The 8 h predicted concentrations are in the range 4602–460 175 $\mu\text{g m}^{-3}$ as shown in Fig. 8. The 24 h predicted concentrations have values in the range 1701–170 106 $\mu\text{g m}^{-3}$ as shown in Fig. 9. The annual predicted concentrations have values in the range 235–23 466 $\mu\text{g m}^{-3}$ as shown in Fig. 10. The maximum concentrations of VOCs in the 1 h, 8 h, 24 h and annual averaging period are 852 130 $\mu\text{g m}^{-3}$, 460 175 $\mu\text{g m}^{-3}$, 170 106 $\mu\text{g m}^{-3}$ and 23 466 $\mu\text{g m}^{-3}$, respectively.

Table 13 Predicted VOC cumulative impacts around the Sokoto-Aiyekale dump site

Receptor	Predicted concentration ($\mu\text{g m}^{-3}$)				% Recommended in FMEnV
	1 h	8 h	24 h	Annual	24 h (160 $\mu\text{g m}^{-3}$)
Sokoto	20 500	5600	2700	368	16.88
Aiyekale	20 500	4602	—	—	—
Abe-Emi	80 500	14 600	5700	650	35.63
Wara	20 500	5600	2700	235	16.88
Airport	20 500	—	—	—	—
Olorunsogo	20 500	4602	—	—	—
Osere	9511	—	—	—	—
Oko Erin	9511	—	—	—	—
Asa-Dam	9511	—	—	—	—
Egbejila	8521	—	—	—	—
Orisumibare	10 500	—	—	—	—

3.4 Impacts of modelled CAPs on air quality

The impacts of each CAP on the air quality of the host environment are herein presented.

VOCs affect the air quality more, due to their higher predicted concentrations as contained in Tables 12 and 13.

3.4.1 Impacts of PM emissions on ambient air quality. The effects of ground-level PM emissions on the host environment's ambient air quality were studied using the most stringent FMEnV and WHO limits. For 600 $\mu\text{g m}^{-3}$ (1 h averaging period) FMEnV standard, the predicted ground level concentrations for all the identified eleven receptors were above the limits with 25.5, 25.5, 84.67, 34.67, 25.5, 25.5, 16.33, 14.74, 14.74, 14.74 and 16.33 fold predicted respectively for Sokoto, Aiyekale, Abe-Emi, Wara, Airport, olorunsogo, Osere, Oke-Erin, asa-Dam, Egbejila and Orisumibare. Also, for 150 $\mu\text{g m}^{-3}$ (24 h averaging period), the predicted concentrations were above the standard (Table 12) for Sokoto, Abe-Emi and Wara with 16.91, 30 and 16.91 fold respectively. Similarly, using WHO standards, 40–60 $\mu\text{g m}^{-3}$ (annual averaging period), the predicted ground level concentrations were above the standard with 8.94, 16.25 and 5.43 fold at Sokoto, Abe-Emi and Wara respectively.

3.4.2 Impacts of VOC emissions on ambient air quality. The effects of VOC ground level emissions on the host environment's ambient air quality were studied using the most stringent FMEnV limits of 160 $\mu\text{g m}^{-3}$ for a 24 hour averaging period. The predicted concentration of VOCs was higher than the standard (Table 13) in the receptor communities (Sokoto, Abe-Emi and Wara) where 16.88, 35.63 and 16.88 fold were predicted respectively.

4. Conclusions

This research has investigated the emissions from the open burning of solid waste at the Sokoto-Aiyekale dump site and the ground level concentrations of criteria air pollutants were estimated using AERMOD. The atmospheric particulate matter deposition study has highly established the fact that anthropogenic activities such as open burning of solid waste produces



heavy metals in large concentrations, which has a negative impact on the environment.

From the results obtained, the following were the conclusion of the study.

(i) The emission inventory for PM and VOCs was in the range 2200.5–2481.1 and 5913.9–6668.0 tons per annum between 2016 and 2020, respectively.

(ii) Particulate characterization shows that Fe had the highest concentration of 67 512.8 and 73 845.5 $\mu\text{g m}^{-3}$ in the wet and dry seasons respectively. The wet and dry deposition fluxes ranged from 7.32 to 11.46 and 38.83 to 88.8 g per m^2 per month, respectively. Deposition velocities of the trace metals were in the range 0.0000528–0.00075444 m s^{-1} and 0.0003377–0.0048183 m s^{-1} in the wet and dry seasons respectively. The scavenging ratio ranged from 0.66 to 3.96 and 0.54 to 2.13 in the wet and dry seasons respectively.

(iii) The daily quality of air was within the Federal Ministry of Environment's (FMEnV) guidelines. Nevertheless, the 1 hour, 24 hour, and annual PM air quality for all receptor communities exceeded the FMEnV and World Bank standards.

(iv) Abe-Emi, Sokoto and Wara communities are at risk of VOC emissions. Also, all the receptor communities are negatively affected by PM emissions.

Conflicts of interest

The authors confirm that there are no disclosures or potential conflict of interest pertaining to this research work and its submission for publication.

Acknowledgements

The authors acknowledge the laboratory staff of the Department of Chemical Engineering, LAUTECH, Ogbomoso for their assistance during the course of this research.

References

- 1 A. Olaide M and G. Dias A, Municipal Solid Waste Characterization as a Measure towards Sustainable Waste Management in Abuja, Nigeria, *J. Environ. Sci. Public Health*, 2020, **4**(2), 43–60.
- 2 P. Lestari, S. Damayanti and M. K. Arrohan, Emission Inventory of Pollutants (CO , SO_2 , $\text{PM}_{2.5}$, and NO_x) in Jakarta Indonesia, in *IOP Conference Series: Earth and Environmental Science*, 2020, vol. 489, no. 1, DOI: [10.1088/1755-1315/489/1/012014](https://doi.org/10.1088/1755-1315/489/1/012014).
- 3 W. Powrie, C. Velis, E. Cook and H. Ingham, Open uncontrolled burning of solid waste undermines human health: Time to act, *Waste Manage. Res.*, 2021, **39**(1), 1–2.
- 4 O. I. Nkwachukwu, N. I. Chidi and K. O. Charles, Issues of Roadside Disposal Habit of Municipal Solid Waste, Environmental Impacts and Implementation of Sound Management Practices in Developing Country 'Nigeria', *Int. J. Environ. Sci. Dev.*, 2010, **1**(5), 409–418.
- 5 S. E. Vergara and G. Tchobanoglous, Municipal solid waste and the environment: A global perspective, *Annu. Rev. Environ. Resour.*, 2012, **37**, 277–309, DOI: [10.1146/annurev-environ-050511-122532](https://doi.org/10.1146/annurev-environ-050511-122532).
- 6 G. Tchobanoglous, F. Kreith, and M. E. Williams, *Integrated Solid Waste Management Engineering Principles and Management Issues*, 1993.
- 7 S. Kaza, L. C. Yao, P. Bhada-Tata and F. Van Woerden, *What a Waste 2.0: A Global Snapshot of Solid Waste Management to 2050*. Urban Development; Washington, DC: World Bank. © World Bank, *What a Waste 2.0*, 2018.
- 8 R. A. Ibikunle, I. F. Titiladunayo, B. O. Akinnuli, S. O. Dahunsi and T. M. A. Olayanju, Estimation of power generation from municipal solid wastes: A case Study of Ilorin metropolis, Nigeria, *Energy Rep.*, 2019, **5**, 126–135.
- 9 H. I. Abdel-Shafy and M. S. M. Mansour, Solid waste issue: Sources, composition, disposal, recycling, and valorization, *Egypt. J. Pet.*, 2018, **27**(4), 1275–1290.
- 10 S. Kumar, J. K. Bhattacharyya, A. N. Vaidya, T. Chakrabarti, S. Devotta and A. B. Akolkar, Assessment of the status of municipal solid waste management in metro cities, state capitals, class I cities, and class II towns in India: An insight, *Waste Manage.*, 2009, **29**(2), 883–895.
- 11 E. Cook and C. Velis, *Global Review on Safer End of Engineered Life*, London, UK, 2021, DOI: [10.5518/100/58](https://doi.org/10.5518/100/58).
- 12 D. R. Boyd, The human right to breathe clean air, *Ann. Glob. Health*, 2019, **85**(1), 146.
- 13 P. Shao, X. Xu, X. Zhang, J. Xu, Y. Wang and Z. Ma, Impact of volatile organic compounds and photochemical activities on particulate matters during a high ozone episode at urban, suburb and regional background stations in Beijing, *Atmos. Environ.*, 2020, **236**, 117629.
- 14 I. C. Yadav and N. L. Devi, Biomass Burning, Regional Air Quality, and Climate Change, in *Encyclopedia of Environmental Health*, Elsevier, 2019, pp. 386–391.
- 15 R. El Morabet, Effects of outdoor air pollution on human health, in *Encyclopedia of Environmental Health*, Elsevier, 2019, pp. 278–286.
- 16 B. Acharya, Cleaning of product gas of gasification, in *Biomass Gasification, Pyrolysis and Torrefaction: Practical Design and Theory*, Academic Press, 2018, pp. 373–391.
- 17 K. H. Kim, E. Kabir and S. Kabir, A review on the human health impact of airborne particulate matter, *Environ. Int.*, 2015, **74**, 136–143.
- 18 J. E. Thompson, Airborne Particulate Matter: Human Exposure and Health Effects, *J. Occup. Environ. Med.*, 2018, **60**(5), 392–423, DOI: [10.1097/JOM.0000000000001277](https://doi.org/10.1097/JOM.0000000000001277).
- 19 Minnesota Department of Health, *Volatile Organic Compounds (VOCs) in Your Home*, Minnesota, 2020.
- 20 United States Environmental Protection Agency, What are volatile organic compounds (VOCs)?, *Indoor Air Qual.*, 2019, <https://www.epa.gov/indoor-air-quality-iaq/what-are-volatile-organic-compounds-vocs>.
- 21 The Environment and Water and Department of Climate Change, Energy, Total Volatile Organic Compounds, Environment, 2022, <https://www.dccew.gov.au/environment/protection/npi/substances/fact-sheets/total-volatile-organic-compounds>, accessed Feb. 14, 2023.



- 22 P. Fusar-Poli, J. A. Crippa, S. Bhattacharyya, S. J. Borgwardt, P. Allen, R. Martin-Santos, M. Seal, S. A. Surguladze, C. O'Carroll, Z. Atakan, A. W. Zuardi and P. K. McGuire, Distinct Effects of D9-tetrahydrocannabinol and Cannabidiol on Neural Activation During Emotional Processing, *Arch. Gen. Psychiatry*, 2009, **24**(S1), 95–105.
- 23 D. A. Vallero, Air pollution dispersion models, in *Air Pollution Calculations*, Elsevier, 2019, pp. 429–448.
- 24 P. H. Ryan and G. K. LeMasters, A review of land-use regression models for characterizing intraurban air pollution exposure, *Inhalation Toxicol.*, 2007, **19**(1), 127–133.
- 25 J. Chen, *et al.*, A review of biomass burning: Emissions and impacts on air quality, health and climate in China, *Sci. Total Environ.*, 2017, **579**, 1000–1034.
- 26 EPA, *Support Center for Regulatory Atmospheric Modeling (SCRAM), Receptor Modeling*, EPA Home, 2016.
- 27 USEPA, Air Quality Criteria for Particulate Matter, *Air Qual. Criteria Part. Matter*, 2004, **1**, <https://www.epa.gov/scram/air-pollutant-receptor-modeling>.
- 28 B. S. Ajadi and A. M. Tunde, Spatial Variation in Solid Waste Composition and Management in Ilorin Metropolis, Nigeria, *J. Hum. Ecol.*, 2010, **32**(2), 101–108.
- 29 I. P. Ifabiyi, Predicting Borehole Yield on the Precambrian Basement Complex and Sedimentary Rocks in West Central Nigeria, in *Review of Growth and Change*, Department of Geography and Planning Sciences, Ondo State University., 1998, no. 2, pp. 7–13.
- 30 J. A. Sonibare, Air pollution implications of Nigeria's present strategy on improved electricity generation, *Energy Policy*, 2010, **38**(10), 5783–5789.
- 31 United States Environmental Protection Agency, AP-42, Compilation of Air Pollutant Emission Factors, in *Pollution Control Handbook for Oil and Gas Engineering*, John Wiley & Sons, Inc., Hoboken, NJ, USA, 2016, pp. 137–140.
- 32 S. A. Adebajo, A. O. Alade, O. Duduyemi, A. O. Adeosun, O. E. Oyeyinka, A. O. Popoola and L. A. Jimoda, Examination of Wet Atmospheric Deposition Fluxes For Odogunyan Industrial Estate in 2015 And 2020, *Int. J. Res. Eng. Sci.*, 2022, **10**(4), 4–10.
- 33 L. A. Jimoda, J. A. Sonibare and F. A. Akeredolu, Wet And Dry Deposition Studies Of Aerosol Hazes Around A Major Sawdust Open Burning Area, *Ife J. Technol.*, 2010, **19**(1), 100–106, <https://ijt.oauife.edu.ng/index.php/ijt/article/view/56>.
- 34 M. Addo, *et al.*, Evaluation of Heavy Metals Contamination of Soil and Vegetation in the Vicinity of a Cement Factory in the Volta Region, Ghana, *Int. J. Sci. Technol.*, 2012, **2**(1), 40–50.
- 35 N. Elom, M. Deary and J. Dean, Determination of trace elements in urban airborne particulates (PM₁₀) using energy dispersive X-ray fluorescence (EDXRF) spectroscopy, *J. Appl. Sci. Environ. Manag.*, 2015, **18**(4), 609, DOI: [10.4314/jasem.v18i4.8](https://doi.org/10.4314/jasem.v18i4.8).
- 36 M. Amodio, S. Catino, P. R. Dambruoso, G. de Gennaro, A. Di Gilio, P. Giungato, E. Laiola, A. Marzocca, A. Mazzone, A. Sardaro and M. Tutino, Atmospheric deposition: Sampling procedures, analytical methods, and main recent findings from the scientific literature, *Adv. Meteorol.*, 2014, **2014**, 1–27.
- 37 Y. M. Amouzouvi, M. M. Dzagli, K. Sagna, Z. Török, C. A. Roba, A. Mereuță, A. Ozunu and K. S. Edjame, Evaluation of pollutants along the national road N₂ in Togo using the AERMOD dispersion model, *J. Health Pollut.*, 2020, **10**(27), 200908.
- 38 L. A. Jimoda, J. A. Adeniran, J. A. Sonibare and A. A. Ayandiran, Investigation of NO₂/NO, SO₂, CO and volatile organic compounds emission from solid waste in Ogbomoso, *Civ. Res. Res.*, 2013, **3**(7), 145–152, <https://www.iiste.org/Journals/index.php/CER/article/view/6127/6256>.
- 39 N. Janssen, *et al.*, Health effects of Black Carbon, *Atmos. Environ.*, 2015, **41**(28), 86.
- 40 S. I. Efe, Particulate Pollution and Its Health Implications in Warri Metropolis, Delta State Nigeria, *Environ. Anal.*, 2006, **11**, 1339–1351.
- 41 M. Mohan, S. Bhati and A. Rao, Application of air dispersion modelling for exposure assessment from particulate matter pollution in mega city Delhi, *Asia-Pacific J. Chem. Eng.*, 2011, **6**(1), 85–94.
- 42 A. S. Nagpure, A. Ramaswami and A. Russell, Characterizing the Spatial and Temporal Patterns of Open Burning of Municipal Solid Waste (MSW) in Indian Cities, *Environ. Sci. Technol.*, 2015, **49**(21), 12904–12912.
- 43 S. Kumar, S. G. Aggarwa, B. Sarangi, J. Malherbe, J. P. G. Barre, S. Berail, F. Séby and O. F. X. Donard, Understanding the influence of open-waste burning on urban aerosols using metal tracers and lead isotopic composition, *Aerosol Air Qual. Res.*, 2018, **18**(9), 2433–2446.
- 44 L. V. Antisari, F. Ventura, A. Simoni, S. Piana, P. R. Pisa and G. Vianelloz, Assessment of Pollutants in Wet and Dry Depositions in a Suburban Area around a Waste-to-Energy Plant (WEP) in Northern Italy, *J. Environ. Prot.*, 2013, **4**(5), 16–25.
- 45 M. Balali-Mood, K. Naseri, Z. Tahergorabi, M. R. Khazdair and M. Sadeghi, Toxic Mechanisms of Five Heavy Metals: Mercury, Lead, Chromium, Cadmium, and Arsenic, *Front. Pharmacol.*, 2021, **12**, 643972.
- 46 S. Mitra, *et al.*, Impact of heavy metals on the environment and human health: Novel therapeutic insights to counter the toxicity, *J. King Saud Univ., Sci.*, 2022, **34**(3), 101865.
- 47 V. Masindi and K. L. Muedi, Environmental Contamination by Heavy Metals, in *Heavy Metals*, 2018.
- 48 D. T. Allen, Combining innovative science and policy to improve air quality in cities with refining and chemicals manufacturing: The case study of Houston, Texas, USA, *Front. Chem. Sci. Eng.*, 2017, **11**(3), 293–304, DOI: [10.1007/s11705-017-1660-0](https://doi.org/10.1007/s11705-017-1660-0).
- 49 H. Yan, X. Liu, J. Qi and H. Gao, Dry deposition of PM₁₀ over the Yellow Sea during Asian dust events from 2001 to 2007, *J. Environ. Sci.*, 2014, **26**(1), DOI: [10.1016/S1001-0742\(13\)60380-0](https://doi.org/10.1016/S1001-0742(13)60380-0).
- 50 D. Zhang, T. S. Keat and R. M. Gersberg, A comparison of municipal solid waste management in Berlin and Singapore, *Waste Manage.*, 2010, **30**(5), 921–933.



- 51 J. Qi, P. Li, X. Li, L. Feng and M. Zhang, Estimation of dry deposition fluxes of particulate species to the water surface in the Qingdao area, using a model and surrogate surfaces, *Atmos. Environ.*, 2005, **39**(11), 2081–2088.
- 52 P. Lestari, A. K. Oskouie and K. E. Noll, Size distribution and dry deposition of particulate mass, sulfate and nitrate in an urban area, *Atmos. Environ.*, 2003, **37**(18), 2507–2516.
- 53 H. J. Yun, S. M. Yi and Y. P. Kim, Dry deposition fluxes of ambient particulate heavy metals in a small city, Korea, *Atmos. Environ.*, 2002, **36**(35), 5449–5458.
- 54 A. O. Alamu, A. O. Alade, S. A. Adebajo and L. A. Jimoda, Elemental Characterization of Aerosols in Wet Deposition along a Dense Traffic Highway in Ogbomoso, Nigeria, *Eng. Technol. Res. J.*, 2020, **5**(1), 7–17.
- 55 A. E. Adeniran, A. T. Nubi and A. O. Adelopo, Solid waste generation and characterization in the University of Lagos for a sustainable waste management, *Waste Manag.*, 2017, **67**, 3–10.
- 56 A. R. Ipeaiyeda and B. A. Falusi, Monitoring of SO₂, NO_x and NH₃ emission from burning of solid wastes at Awotan and Lapite dumpsites, Ibadan, Nigeria, *South African J. Chem.*, 2018, **71**, 166–173.
- 57 B. S. Fakinle, E. L. Odekanle, A. P. Olalekan, H. E. Ije, D. O. Oke and J. A. Sonibare, Air pollutant emissions by anthropogenic combustion processes in Lagos, Nigeria, *Cogent Eng.*, 2020, **7**(2), 1808285.
- 58 R. E. Daffi, A. N. Chaimang and M. I. Alfa, Environmental Impact of Open Burning of Municipal Solid Wastes Dumps in Parts of Jos Metropolis, Nigeria, *J. Eng. Res. Reports*, 2020, 30–43, DOI: [10.9734/jerr/2020/v12i317083](https://doi.org/10.9734/jerr/2020/v12i317083).
- 59 J. Pansuk, A. Junpen and S. Garivait, Assessment of air pollution from household solid waste open burning in Thailand, *Sustainability*, 2018, **10**(7), 2553.

